

# First Year Report - Draft

Oliver S Burren

August 14, 2016

## **Abstract**

TODO

# Contents

<b>1</b>	<b>Introduction</b>	<b>3</b>
1.1	Motivation . . . . .	3
1.2	Fine mapping . . . . .	4
1.3	Variant set enrichment . . . . .	6
1.4	High resolution promoter capture Hi-C . . . . .	7
<b>2</b>	<b>Materials and Methods</b>	<b>8</b>
2.1	Promoter capture interaction maps of 17 haematopoietic primary human cells . . . . .	8
2.2	Collection and quality control of GWAS summary statistics from 31 genome wide association studies . . . . .	8
2.3	Poor Man's Imputation (PMI) - Imputation of GWAS p-values to the 1000 Genome reference panel in the absence of effect size and direction . . . . .	9
2.4	Causal variant posterior probabilities for 31 traits using GWAS summary statistics	9
2.5	Comparison of posterior probabilities between PMI and classical imputation . . . . .	10
2.6	Causal variant posterior probabilities for using ImmunoChip summary statistics . . . . .	10
2.7	blockshifter - A competitive test for associated variant enrichment in PCHiC interaction maps . . . . .	10
2.8	COGS - An algorithm for PCHiC assisted prioritisation of genes and tissues contexts . . . . .	11
2.9	Comparison of COGS scores to non PCHi-C methods . . . . .	13
2.10	Enrichment of COGS in disease specific differentially expressed genes . . . . .	14
<b>3</b>	<b>Results</b>	<b>15</b>
3.1	Comparison of PM with genotype level imputation . . . . .	15
3.2	Tissue specific enrichment of associated variants with PIRs across 31 traits . . . . .	15
3.3	PCHiC assisted gene prioritisation across 31 traits . . . . .	15
3.4	Tissue specific PCHiC assisted gene prioritisation using dense summary statistics	16
3.5	Comparison of COGS with TAD bounday prioritisation . . . . .	17
3.6	Prioritised gene overlap with eQTLs . . . . .	17
3.7	COGS prioritisation qualitatively performs better than TAD and distance based scores . . . . .	18

3.8 COGS prioritised genes are enriched for disease specific differentially expressed genes . . . . .	19
<b>4 Discussion</b>	<b>25</b>
4.1 Functional validation of COGS prioritised gene <i>IL2RA</i> . . . . .	25
4.2 Limitations . . . . .	25
<b>5 Future Work</b>	<b>29</b>
5.1 Application of COGS scores to the full PCHiC dataset . . . . .	29
5.2 Comparison with Hi-C defined TAD boundaries . . . . .	29
5.3 Integrating other annotations into COGS . . . . .	29
5.4 blockshifter development - perhaps omit . . . . .	31
5.5 Tissue specific gene set enrichment analysis . . . . .	31
5.6 Data driven discovery of relevant COGS score thresholds . . . . .	31
5.7 Future Directions . . . . .	31

# Chapter 1

## Introduction

### 1.1 Motivation

A key property of the adaptive immune system is the ability to recognise pathogens from self-antigens. Dysregulation of this process results in damage to healthy tissues and autoimmunity. Currently, over 80 diseases have been found to have an underlying autoimmune pathogenesis, with approximately half presenting as rare diseases [Hayter and Cook, 2012]. The health burden of more common autoimmune diseases such as type 1 diabetes (T1D), rheumatoid arthritis (RA), inflammatory bowel disease (IBD) and multiple sclerosis (MS) is high with approximately 7 - 9% of the European population affected [Cooper et al, 2009]. Although environment is a contributing factor in disease susceptibility, the genetic heritability, defined as the proportion of phenotypic variance attributable to genetic variability, ranges from 0.39 in primary biliary cirrhosis (PBC) to 0.9 in ankylosing spondilitis (AS) [Gutierrez-Arcelus et al, 2016].

Genome wide association studies (GWAS) have been instrumental in understanding the the genetic architecture underlying autoimmune disease susceptibility with at least 324 distinct genetic loci robustly associated with one or more autoimmune diseases (<http://www.immunobase.org>, accessed 01/08/2016). Focus is now drawn to elucidating the mechanisms by which causal variation modulates phenotypic endpoints, a prerequisite for successful therapeutic development. Interestingly, the majority of associated variants fall outside of genes [Maurano et al, 2012] and the integrative analysis of chromatin marks with GWAS highlights a tissue specific specific regulatory role [Farh et al, 2015]. Recent studies [Claussnitzer et al, 2015; Davison et al, 2012; Smemo et al, 2014] have shown that such regulatory variants might, through chromatin conformation, regulate distal genes. However, further progress in this area has been hampered by incomplete knowledge of causal variants and their target genes and the specific tissue contexts in which they operate [Albert and Kruglyak, 2015].

To date systematic methods for incorporating physical interactions between variants and their target genes have not been attempted. In this report I describe tools and analytical methods to integrate genetic and high resolution promoter capture Hi-C (PCH-C). Such methods provide a data driven approaches to prioritising putative causal variants underlying autoimmune disease susceptibility, relevant tissue contexts, genes and biological pathways. To do this

I develop fine mapping, variant set enrichment and pathway analysis methods that use PHi-C data from 17 primary human cell types to analyse GWAS data across 10 autoimmune and 23 non-autoimmune traits.

## 1.2 Fine mapping

One of the first steps of this project is to identify optimal methods for fine mapping, that balance data availability, resolution and computational efficiency. Fine mapping is the process of refining association signals in a genomic region in order to characterise fine scale genetic architecture, a necessary step in order to identify putative causal variants. Progress in this area is challenging, due to the presence of linkage disequilibrium (LD), which in many cases means that the causal variation cannot be resolved statistically with current sample sizes.

One approach, under the simplifying assumption that a single causal variant explains the effect within a given genetic region, is to apply Wakefield's synthesis of approximate Bayes Factors (ABF) [Wakefield, 2009] to each variant within the region. These can be converted into posterior probabilities for a SNP to be causal using methods described in The Wellcome Trust Case Control Consortium et al [2012]. A sizeable benefit of this approach is that it circumvents privacy issues, as the input is limited to GWAS summary statistics rather than access to full genotyping data.

Wakefield defines the ABF as

$$ABF = \sqrt{1 - r} \times \exp \left[ \frac{Z^2}{2} \times r \right] \quad (1.1)$$

If a given set of summary statistics include  $\hat{\beta}$ , an our estimate of the log(Odds Ratio) and  $\sqrt{V}$ , the standard error of the Odds Ratio for a variant, then we can compute a  $Z$  score such that  $Z = \frac{\hat{\beta}}{\sqrt{V}}$ . Alternatively, if only univariate  $p$ -values are supplied a  $Z$  score can be estimated using an inverse normal cumulative distribution function . If  $r$ , a shrinkage factor, is defined as the the ratio of the prior variance on  $\hat{\beta}$  to the total variance, then,  $r = \frac{W}{V+W}$ .  $V$  is approximated using the variant minor allele frequency (MAF) and study sample size such that  $V = \frac{1}{2Nf(1-f)}$  for quantitiative traits, where  $N$  is number of samples and  $f$  is the MAF. In the case/control setting  $V = \frac{1}{2Nf(1-f)s(1-s)}$  where  $s$  is the proportion of cases . The value of  $\sqrt{W}$ , the standard deviation of a normal prior, depends on study design considerations. In this report we use values of 0.15 and 0.2 for case/control and quantitative trait settings respectively, as discussed by Giambartolomei et al [2014].

Given the ABF for all SNPs in a given genetic block we can estimate the posterior probability

that a SNP  $i$  is causal using the following.

$$\begin{aligned}
PP_i &= P(\text{SNP}_i \text{ causal} | D) \\
&= \frac{P(D|\text{SNP}_i \text{ causal})\pi_i}{\sum_j P(D|\text{SNP}_j \text{ causal})\pi_j + P(D|H_0)\pi_0} \\
&= \frac{\frac{P(D|\text{SNP}_i \text{ causal})}{P(D|H_0)}\pi_i}{\sum_{j=1}^n \frac{P(D|\text{SNP}_j \text{ causal})}{P(D|H_0)}\pi_j + \pi_0} \\
&= \frac{\text{BF}_i \pi_i}{\sum_{j=1}^n \text{BF}_j \pi_j + \pi_0} \\
&\approx \frac{\text{BF}_i \pi_i}{\sum_{j=1}^n \text{BF}_j \pi_j + 1}
\end{aligned} \tag{1.2}$$

Note that as  $\pi_0 = 1 - \sum_j \pi_j \approx 1$ .

$\pi_i$  is our prior probability for any SNP selected at random to be causal for a trait. Current sample sizes are underpowered and therefore have limited resolution. This has driven the development of integrative techniques that couple fine mapping methods with functional information to further prioritise causal variants. Examples include *fgwas* [Pickrell, 2014], PAINTOR [Kichaev et al, 2014], RiVIERA [Li and Kellis, 2016] and the integration of eQTL data sets using Mendelian randomisation [Zhu et al, 2016]. As an example Pickrell [2014] developed a Bayesian hierarchical frameworks implemented in *fgwas* that estimates variable priors for each SNP based on other sources of annotation. For a given SNP the prior probability for association,  $\pi_{ik}$ , varies depending on the enrichment of annotations,  $\lambda_l$ .

$$\pi_{ik} = \frac{e^{x_i}}{\sum_{j \in S_k} e^{x_j}} \tag{1.3}$$

$x_i$  is the sum of the effect of all the annotations that the  $i^{th}$  SNP overlaps as shown below. Here  $\lambda_l$  is the effect of annotation  $l$  and  $I_{il}$  is an indicator function as to whether SNP  $i$  overlaps annotation  $l$ .

$$x_i = \sum_{l=1}^{L_2} \lambda_l I_{il} \tag{1.4}$$

$\lambda_l$  is itself of interest as it indicates whether a given annotation is enriched for association with a trait of interest. When combined with equation 1.2  $\pi_{ik}$  allows the incorporation of functional information with genetic data allowing a modest increase in resolution and a resultant decrease in the number of causal SNPs to be considered. Whilst promising *fgwas* requires careful cross-validation to prevent overfitting whereby the derived model is biased for the training set but performs poorly on a test set of data, and all such methods are limited by the annotations available.

If raw genotyping data for a study is available then stepwise regression could be used, however whilst this approach is attractive computationally, doubts exist over its validity [Miller,

1984]. Effectively having selected a single variant that best explains the variance of a trait, stepwise regression then looks for other variants that explain additional trait variance conditional on this ‘top’ variant. This is not equivalent to explaining which variants jointly explain the variance of a trait. However, approaches that search the model space exhaustively are only computationally feasible for simple models incorporating a limited number of variants. An alternative approach is to use Monte Carlo methods to sample the model space allowing the consideration of multiple causal variants within a genetic region. One example is GUESSFM that uses a Bayesian evolutionary stochastic search algorithm to effectively sample the model space, and has been shown to have consistently better performance when variants are highly correlated Wallace et al [2015].

### 1.3 Variant set enrichment

The next part of my project investigates whether the putative causal SNPs identified can be used to better understand the biology of autoimmune disease. If these variants are enriched for a particular annotation or gene set then this can provide global information on mechanisms, relevant tissue contexts and biological pathways. However this is complicated by both correlation between variants (due to linkage disequilibrium) and annotations.

$$\text{Var}(A + B) = \text{Var}(A) + \text{Var}(B) + 2\text{Cov}(A, B) \quad (1.5)$$

If  $A$  and  $B$  are non independent variables then the covariance term  $2\text{Cov}(A, B)$  can be almost as large as  $\text{Var}(A) + \text{Var}(B)$ . This causes the observed variance to be inflated compared to the theoretical variance if independence is assumed. Unfortunately most classical statistical tests based on linear sums of variables assume independence and thus the inflated variance of the computed test statistic increases type 1 error, that is the erroneous rejection of the null hypothesis. Permutation based methods, that can use GWAS summary statistics are desirable as they can help to overcome this inflation by estimating the variance empirically. There are two broad permutation methods, firstly, using a suitable reference genotype set to compute covariance matrices allows the estimation of SNP variance under the null hypothesis using the multivariate normal Burren et al [2014]; Liu et al [2010]. These approaches are computationally expensive and scale exponentially with SNP density, thus an LD pruning strategy is employed which limits resolution and therefore is only applicable to larger genomic annotations such as genes. The second approach is to permute the annotations over the SNPs whilst maintaining the spatial correlation structure of the target annotation to estimate the variance under the null. The latter approach is attractive as it favours high resolution annotations and is computationally more tractable. GOSHIFTER is a recent implementation using a circular permutation strategy [Trynka et al, 2015] that demonstrates this approach finding enrichment for H3K4me3 marks in CD+ memory T cells.

As previously mentioned integrative approaches such as *fgwas* combine variant set enrichment with fine mapping strategies to simultaneously prioritise annotations and variants. This

approach additionally benefits from jointly assessing multiple annotations, thus if there is additional correlation between different annotation types this can be adjusted for. It should be noted that all methods are dependent on the quality and coverage of input annotations. A recent study fine mapping IBD causal variants found that 21 variants with extremely high probability ( $> 95\%$ ) to be causal did not overlap any functional annotations, drawing attention to the inadequacies of current genomic functional annotation [Huang et al, 2015a].

## 1.4 High resolution promoter capture Hi-C

The most novel aspect of this project is using a data driven approach to link putative causal variation to the target genes in relevant tissues. Techniques such as Hi-C [Lieberman-Aiden et al, 2009] and Chromatin Interaction Analysis by Paired-End Tag Sequencing (ChIA-PET) [Fullwood et al, 2009] have been developed to map the genome-wide chromatin interactions in specific cell types [Rao et al, 2014]. Hi-C involves cross-linking genomic DNA with formaldehyde resulting in covalent links between spatially adjacent chromatin segments. This chromatin is then digested with a restriction enzyme and sticky ends are filled in with biotin labelled nucleotides. Ligation is then performed under dilute conditions which favours intramolecular ligation events. The DNA is then purified and then sonically sheared and fragments are then enriched for biotinylated junctions, which then undergo paired end sequencing [van Berkum et al, 2010]. ChIA-PET again involves using formaldehyde to covalently link spatially adjacent chromatin. After sonification an immunoprecipitation step is used to select a protein of interest (e.g. transcription factor) and the chromatin to which it is bound. Next biotin conjugated linker sequences are ligated to the free ends of the immunoprecipitated DNA. A further proximity based ligation takes place with enrichment of biotinylated linkers. Barcodes within the linker sequences are used to resolve chimeric intra and inter complex interactions.

Whilst both are genome-wide methods for interrogating chromatin looping, ChIA-PET targets a specific protein and therefore compared to Hi-C is unable to give an unbiased overview of all chromatin interactions within a given tissue context. However, Hi-C resolution is limited by two main factors. Firstly the protocol involves a restriction enzyme digest, usually *HindIII*, and interactions are called based on the resultant fragments generated, in practice if *HindIII* is used this limits resolution to approximately 4Kb. Secondly, the complexity of the sequence libraries generated means that to increase the effective resolution of conventional Hi-C by a factor  $n$  requires  $n^2$  sequencing reads which is prohibitive for general implementation [Jäger et al, 2015]. Promoter capture Hi-C (PCHi-C) incorporates a sequence capture extension to classical Hi-C to enrich for chromatin interactions with protein coding gene promoters [Mifsud et al, 2015]. Such PCHi-C allows for increasing resolution in an approximately linear fashion with increased sequence depth allowing for an economically viable approach for identifying promoter interactions.

# Chapter 2

## Materials and Methods

### 2.1 Promoter capture interaction maps of 17 haematopoetic primary human cells

I obtained maps of 17 primary human cells of the haematopoetic lineage that were generated collaboratively with members of the Fraser, Spivakov, Ouwehand and Diabetes and Inflammation Laboratories. Each cell type was assessed over on average 3 technical replicates (Table 1). The bespoke capture platform employed encompassed a total of 22,076 *HindIII* fragments containing 31,253 annotated promoters for 18,202 protein-coding and 10,929 non-protein coding genes (Ensembl v75). Significantly interacting regions were called using the CHiCAGO pipeline [Cairns et al, 2016]. Interactions with a CHiCAGO score threshold of  $\geq 5$  were used in all downstream analysis. These maps consist of a bait *HindIII* fragment and a list of interacting *HindIII* fragments or promoter interacting regions (PIR) within a particular cellular context.

### 2.2 Collection and quality control of GWAS summary statistics from 31 genome wide association studies

I downloaded GWAS summary statistics, covering 8 autoimmune and 23 other traits, from online resources, as detailed in Table 2. Genotyping error can create false associations, therefore I filtered all association statistics to include only robust associations by removing those SNPs which were genome-wide significant ( $p < 5 \times 10^{-8}$ ) but for which no variants, within 500Kb, in LD ( $r^2 > 0.6$ ) with the lead SNP had  $p < 1 \times 10^{-5}$ . Finally I removed any SNP that was genome-wide significant but was not found in the 1000 Genomes Phase III EUR genotype set.

### **2.3 Poor Man’s Imputation (PMI) - Imputation of GWAS p-values to the 1000 Genome reference panel in the absence of effect size and direction**

There was a high degree of variation in the coverage of GWAS summary statistics obtained, some studies contained information on approximately  $5 \times 10^5$  variants where as others were imputed to 1000 genome reference genotype set and contained in excess of  $7 \times 10^6$  variants. Imputation can be used to compute approximate association statistics for missing variants however it requires access to underlying genotype data which in this case was unavailable for most traits. Methods exist for imputing summary statistics in the absence of genotyping data such as *GCTA* [Yang et al, 2011] and *IMPG* [Pasaniuc et al, 2014], however these rely on access to odds ratio or  $\beta$  coefficients and their standard errors to estimate direction of effect which are not always available. I therefore designed an alternative ‘best guess’ method, poor man’s imputation (PMI), which requires evaluation but allows the processing of a wide range of traits for which variant coverage is heterogeneous and only univariate  $p$  values are available.

The pipeline I developed, approximates the  $p$ -value for missing SNP summary statistics for a given study using a suitable reference genotype set. Firstly the genome is split into regions based on a recombination frequency of 0.1cM using HapMap recombination rate data. For each region we retrieve from the reference genotype set (1000 genomes EUR cohort) all SNPs that have MAF > 1% and use these to compute pairwise LD. The pipeline pairs each SNP with missing  $p$ -values to the SNP with maximum pairwise  $r^2$ ,  $r^2_{max}$ , if that  $r^2_{max} > 0.6$ , and impute the missing  $p$ -value as that at the paired SNP. SNPs with missing data or without a pair above threshold are discarded as are SNPs that are included in the study but do not map to the reference genotype set.

### **2.4 Causal variant posterior probabilities for 31 traits using GWAS summary statistics**

To fine map candidate causal variants I used Wakefield’s synthesis of approximate Bayes factors (ABF) [Wakefield, 2009] and using the method described in The Wellcome Trust Case Control Consortium et al [2012] computed posterior probabilities for each SNP within 0.1 cM regions, using R code adapted from the *coloc* package [Giambartolomei et al, 2014].

I set the value of prior of the  $i^{th}$  variant being causal ( $\pi_i$ ) to that from Giambartolomei et al [2014],  $10^{-4}$ , which means that we expect 1 in 10,000 SNPs to be causal for a trait. This framework assumes a model where either no SNPs are causal within a region or that exactly one SNP is causal. We masked the MHC region (GRCh37:chr6:25-35Mb) from all downstream analysis due to its extended LD and known strong and complex association with autoimmune diseases

## 2.5 Comparison of posterior probabilities between PMI and classical imputation

Before using PMI posterior probabilities in further analyses it was necessary to assess whether they approximated posterior probabilities derived from classical imputation. Firstly I selected all SNPs mapping to Chromosome 1 as a representative sample. To create a simulated non-imputed data set I pruned these results to contain only SNPs for which p-values were reported in Stahl et al [2010]. I next ran PMI on this pruned data set and using *bedtools* [Quinlan, 2014], merged these with actual the imputed p-values from Okada et al [2014]. I confined my comparison to those SNPs imputed by PMI, a total of 235,412 SNPs

## 2.6 Causal variant posterior probabilities for using ImmunoChip summary statistics

Focusing on Autoimmune traits, I downloaded ImmunoChip summary statistics for six traits from <http://www.immunobase.org> carrying out QC as previously described. The ImmunoChip is a targeted genotyping platform for dense coverage of approximately 180 regions with robust demonstration of association with one or more autoimmune traits [Cortes and Brown, 2011]. Summary statistics for ulcerative colitis, Crohn's disease and psoriasis were supplied privately by study authors. I fine mapped these traits using the PMI method previously described, but replacing 0.1cM regions with the 179 regions (median size 227Kb with an inter quartile range of between 126Kb and 392Kb) that were densely genotyped on the ImmunoChip [Onengut-Gumuscu et al, 2015].

To evaluate my PMI approach I used a set of marginal posterior probabilities of inclusion across four diseases(autoimmune thyroid disease, celiac disease , rheumatoid arthritis and type 1 diabetes) generated by Chris Wallace for which we had access for full genotyping data from ImmunoChip using a stochastic search method that allows for multiple causal variants within a region [Wallace et al, 2015]. I incorporated these into further analysis on the assumption that full genotyping data and imputation would provide more accurate posterior probabilities.

## 2.7 blockshifter - A competitive test for associated variant enrichment in PCHiC interaction maps

In order to examine the enrichment of GWAS signals in promoter interacting regions (PIRs) I developed a method based on ideas implemented in *GOSHIFTER* [Trynka et al, 2015] to examine the enrichment of GWAS signals in the promoter interacting regions (PIR) in order to overcome linkage disequilibrium (LD) and interaction fragment correlation. *blockshifter* implements a competitive test of enrichment between a test set of PIRs compared to a control set. Firstly the coordinates of the PIRs in the union of test and control sets are retrieved, and PIRs with no GWAS signal overlap are discarded. As the test is competitive between PIRs in test

and control sets, those overlapping both are not informative and therefore are excluded from further analysis. For the remaining PIRs we store the number and sum of overlapping GWAS posterior probabilities and these are used to compute  $\delta$ , the difference in the means of posterior probabilities between the test and control set . Due to correlation between GWAS signals and between PIRs the variance of  $\delta$  is inflated we thus compute it empirically using permutation. Runs of one or more PIRs (separated by at most one *HindIII* fragment) are combined into blocks, that are labeled unmixed (either test or control PIRs) or mixed (block contains both test and control PIRs). Unmixed blocks are permuted in a standard fashion by reassigning either test or control labels randomly across blocks taking into account the number of blocks in the observed sets. Mixed blocks are permuted by effectively circularising each block and rotating the labels (figure2.1). I store the mean posterior probabilities across each possible permuted block. The number of choices at each block is small, but there are many blocks. I then randomly sample from each these precomputed block permutations  $n$  times so that the proportion of underlying PIRs labels is the same as the observed set and use this to compute the set of  $\delta_{null}$ . We use  $\delta_{null}$  to compute an empirical  $Z$ -score:

$$Z = \frac{\delta - \bar{\delta}_{null}}{\sqrt{V^*}} \quad (2.1)$$

Where  $V^*$  is an empirical estimate of the variance of  $\delta_{null}$ .

## 2.8 COGS - An algorithm for PCHiC assisted prioritisation of genes and tissues contexts

Whilst the blockshifter method provides information about relevant tissue contexts, the primary goal of this project was to use the PCHi-C information to link causal variation to target gene(s). To do this I developed an algorithm to compute tissue specific gene scores for each GWAS trait, taking into account linkage disequilibrium, interactions and functional SNP annotation (figure2.2). For each gene annotation, for which we have at least one significant interaction and for every nearby recombination block, the algorithm computes a block gene score that is composed of three components.

1. The contribution due to coding SNPs in the annotated coding gene as computed by VEP
2. The contribution due to promoter SNPs, which I define as SNPs that overlap the bait and its pair of flanking *HindIII* fragments and not any coding SNPs.
3. The contribution due to SNPs that overlap interacting other ends for a tissue or set of tissues that do not overlap coding SNPs.

For a given target gene and recombination block the algorithm derives a block gene score that is the sum of the posterior probabilities of SNPs overlapping each component, which is the

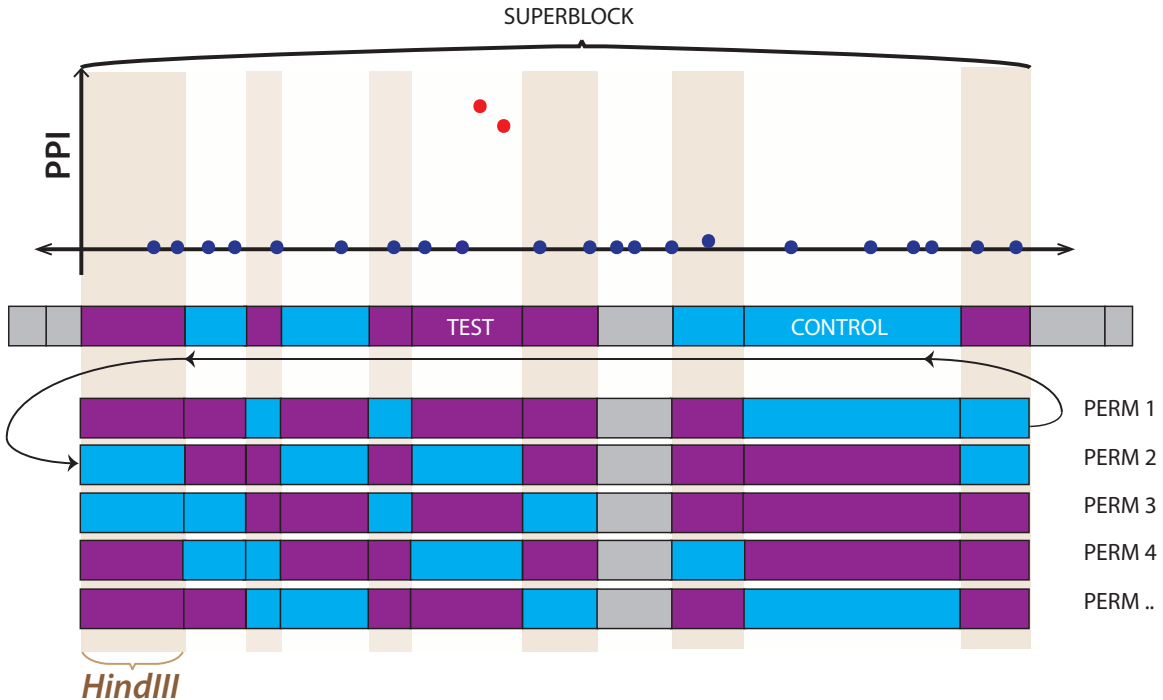


Figure 2.1: Illustration of circularised permutation method for mixed ‘superblocks’. Test(Purple) and Control(Turquoise) tissue PIRs are rotated to generate permutations, *HindIII* fragments with no PIRs (grey) are fixed.

probability that there exists a causal variant for this gene in this block, under the assumption that there is at most one causal variant in any block. Assuming independence we can combine blocks to get an overall gene score such that:

$$\text{Gene score} = 1 - \prod_j \left( 1 - \left( \sum_{i \in R_j} 1 - PP_i \right) \right) \quad (2.2)$$

Here  $PP_i$  is the posterior probability for the  $i^{th}$  variant,  $i \in R_j$  is the set of relevant SNPs  $i$  in the  $j^{th}$  region. Whilst components 1 and 2 are fixed for a given gene and trait the contribution of variants overlapping PIRs varies depending on the tissue context being examined. I developed a hierarchical heuristic method to ascertain for each target gene which was the mostly likely component and cell state. Firstly for each gene I compute the gene score due to genic effects (components 1 + 2) and interactions (component 3) using all available tissue interactions for that gene. I use the ratio of gene effects score to interactions score in a similar manner to a Bayes factor to decide whether one is more likely. If gene effect is more likely (ratio  $> 3$ ) I iterate and compare if the gene score due to coding variants (component 1) is more likely than for promoter variants (component 2). Similarly if an interaction is more likely I compare interaction gene scores for one set of tissue(s) to another. If at any stage no branch is substantially preferred

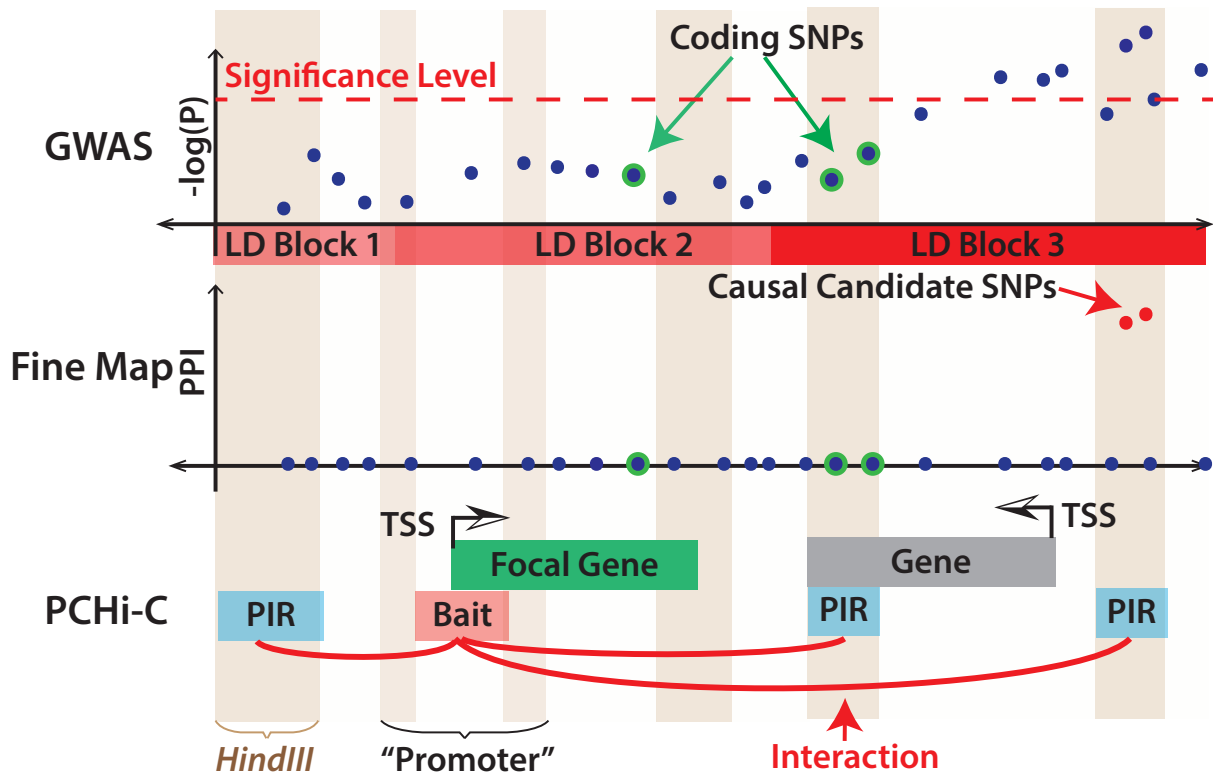


Figure 2.2: Illustration of COGS method

over its competitor (ratio of gene scores  $< 3$ ) I return the previous set as most likely, otherwise I continue until a single cell state/set is chosen. In this way I can prioritise genes based on the overall score and label a likely mechanism for candidate causal variants (5.1).

For the four traits where a stochastic search method was employed I adapted COGS to work with multiple models by aggregating the posterior probabilities for each model with a variant overlapping the PIRs, promoters or coding variants to compute marginal posterior probabilities of inclusion.

## 2.9 Comparison of COGS scores to non PCHi-C methods

To assess the utility of COGS scores and whether PCHi-C datasets were adding information, I generated comparative scores using two other methods orthogonal to PCHi-C. The intent behind this analysis is to assess the utility of interaction data and therefore as input to all methods I supplied PMI datasets from which I had masked coding variation and variation mapping the MHC region on chromosome six. Firstly, I had access to topological associated domain (TAD) boundary information, supplied by Csilla Varnai, Michiel Thieke and Mikhail Spivakov for six cell types (Table ??). I integrated these with the recombination block data used to compute posterior probabilities and used a similar scheme to COGS to compute scores for each TAD and tissue context. I next assigned TAD scores to genes on the basis of TAD and baited gene

fragment overlap. I combined across tissues by taking the maximum score for a given gene across all the tissues. Secondly, I implemented a naive approach taking all *Hind*III within a  $\pm 0.5$  Mb region of a baited gene fragment. I combined these with recombination fragments and then derived scores using a similar method to that implemented for computing TAD scores. Finally I computed a comparison COGS score using only tissues for which TAD boundary information was available.

Tissue	TAD Coverage (Gb)
Erythroblasts	1.53
Macrophages	1.68
Megakaryocytes	1.59
Monocytes	1.48
Naive B cells	1.51
Naive CD4 <sup>+</sup> T cells	1.40
Naive CD8 <sup>+</sup> T cells	1.51
Neutrophils	1.27

Table 2.1: Topologically associated domain coverage across eight cell types elucidated from classical Hi-C analysis

## 2.10 Enrichment of COGS in disease specific differentially expressed genes

As a naive method to assess the biological relevance of the genes prioritised by COGS and to allow quantitative comparison between the TAD, Proximity and COGS methods, I examined genes differentially expressed genes from Peters et al [2016] for enrichment of the different scores. To do this I used differential expression analysis supplied by Chris Wallace. The dataset consists of PEER normalised microarray expression values across 49 patients with Crohn’s disease, 42 with ulcerative colitis and 43 healthy controls, across sorted CD4<sup>+</sup> T cells, CD8+ T cells, B cells, monocytes, and neutrophils. Differential expression was computed with a null hypothesis that expression for a given gene was the same across all three groups within a tissue with two degrees of freedom. COGS and TAD scores were derived by combining over cell types so we did the same, and selected the tissue with the maximum significant differential expression values across tissue for a given gene. As the differential expression analysis concerned ulcerative colitis we included COGS scores generated using GWAS statistics from Anderson et al [2011] and Franke et al [2010] with coding and MHC variants removed.

# Chapter 3

## Results

### 3.1 Comparison of PM with genotype level imputation

To validate performance of the PMI technique, I compared the results as imputed by PMI to those as reported by [Okada et al, 2014]. There was good agreement between PMI imputed p-values and those derived from classical imputation as reported in Okada et al [2014] ( $\rho = 0.9418103$ , figure3.1).

### 3.2 Tissue specific enrichment of associated variants with PIRs across 31 traits

Enrichment of GWAS signals in tissue specific enhancers has been previously described [Maurano et al, 2012] and as we expect PIRs to be enriched for regulatory regions, demonstration of robust enrichment within tissue specific PIRs is a pre-requisite for further analysis that attempts to link causal variation to target genes in relevant tissue contexts. Using *blockshifter* with the PMI imputed summary statistics from the 31 GWAS assembled (Table2), I found that variants associated with autoimmune disease are enriched in PIRs in lymphoid compared to myeloid tissues (figure 3.2). In contrast, SNPs associated with erythroid traits, including mean haemoglobin concentration (MCH), mean corpuscular volume (MCV) and red blood cell count (RBC) showed a selective enrichment in erythroblasts and megakaryocytes compared to PIRs in monocytes, macrophages and neutrophils (figure 3.2). I next examined whether I could further resolve tissue differences using *blockshifter*. I found that autoimmune traits were enriched in activated and non-activated CD4<sup>+</sup> T cells when compared to megakaryocytes and erythroblasts. This enrichment for autoimmune disease traits was stronger in activated compared to non activated CD4<sup>+</sup> T cells (figure 3.3).

### 3.3 PCHiC assisted gene prioritisation across 31 traits

Using COGS, I prioritised 2,604 unique genes (Overall COGS score > 0.5) across all 31 traits examined. The prioritised genes exhibited enrichments for specific pathways in the Reactome

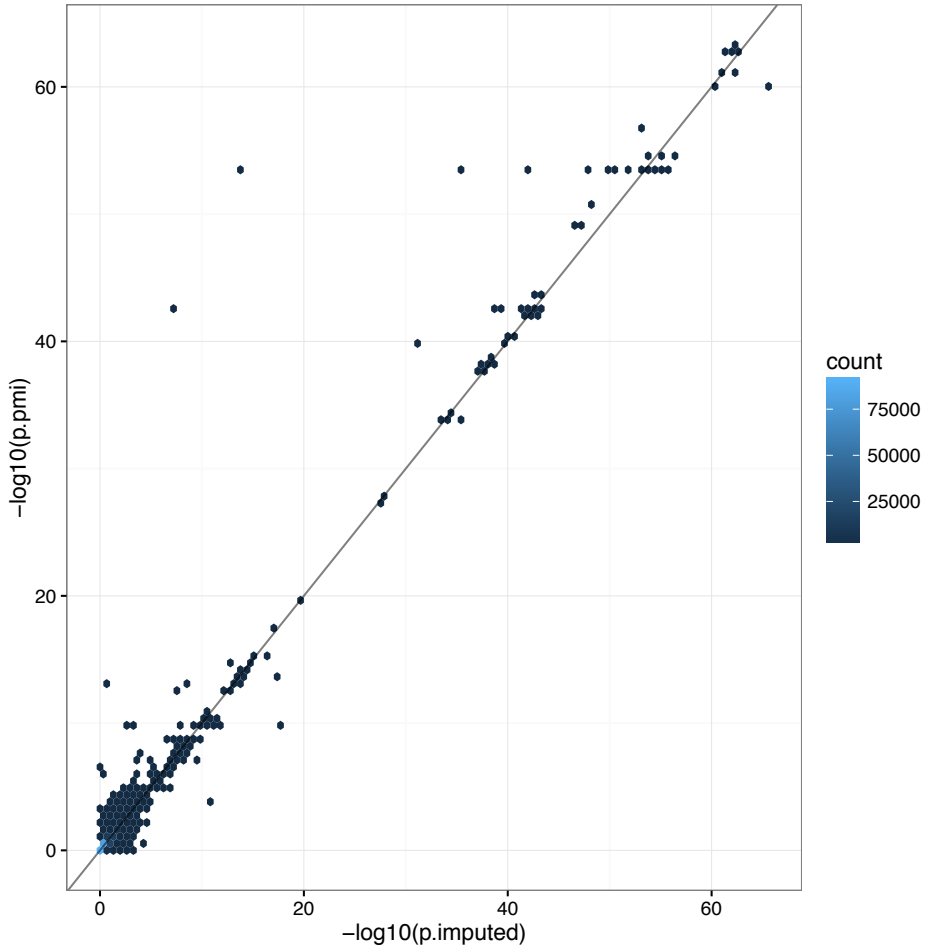


Figure 3.1: Comparison of  $P$ -values imputed by PMI versus those reported in [Okada et al, 2014] for chromosome. Axis are  $-\log_{10}$  transformed  $P$ -values

pathway database [Fabregat et al, 2016]. As expected, genes prioritised for autoimmune diseases were enriched in inflammation and immune response-related pathways, such as interleukin and T cell receptor signalling, whereas genes prioritised for platelet traits were preferentially associated with platelet production and hemostasis (figure??). SNPs associated with traits generally unrelated to haematopoietic cells, such as blood pressure and bone mineral density did not show enrichment for PIRs in any of the cell types analysed.

### 3.4 Tissue specific PCHiC assisted gene prioritisation using dense summary statistics

The stronger enrichment of autoimmune disease GWAS traits in activated CD4 $^{+}$  T cells lead us to examining autoimmune traits in the context of activated and non activated CD4 $^{+}$  promoter interaction maps. We extended COGs to incorporate a simple binary decision tree model to allow tissue or functional category resolution (see methods). Across the combined GWAS and ImmunoChip autoimmune data sets I was able prioritise 602 distinct protein coding genes

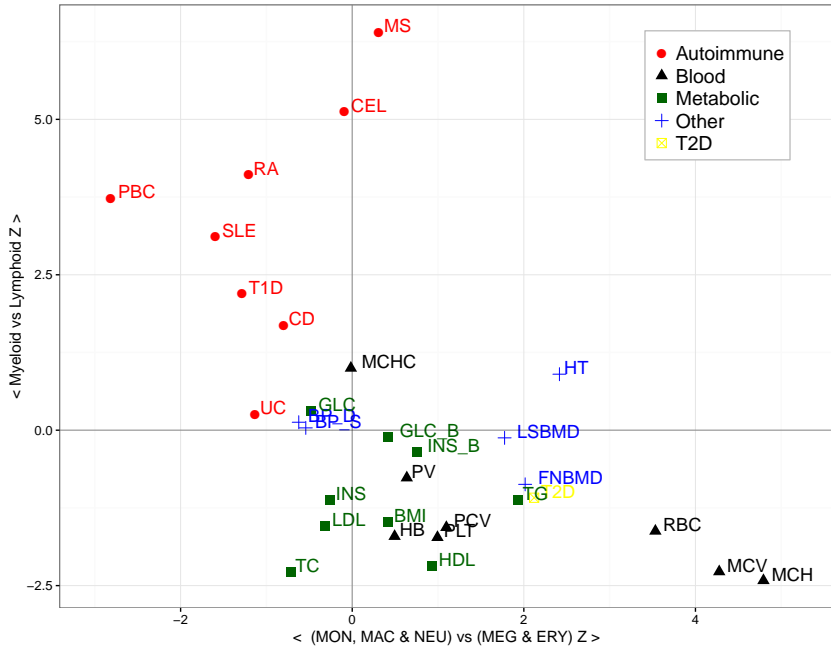


Figure 3.2: Enrichment of GWAS summary statistics at PIRs by tissue groups. Axes reflect *blockshifter*  $Z$ -scores for two different tissue group comparisons, firstly lymphoid versus myeloid and then within myeloid lineage (MON - Monocyte, MAC - macrophage and NEU - Neutrophil) versus (MEG - Megakaryocyte and ERY - erythroblast). Traits are labelled and coloured by category (see appendix ?).

(Figure 3.4). To summarise the behaviour of prioritisation, I focused on a subset of 220 input autoimmune GWAS regions with genome-wide significant signals ( $P < 5 \times 10^{-8}$ ). I prioritised at least one gene with a COGS scores  $> 0.5$  in 122 of these regions, with a median of two genes/region (inter quartile range = 1-3). The average distance from peak signal to prioritised genes was 334 kb and I observed a median of three genes ‘skipped’ between GWAS signal peaks and prioritised genes. Using pooled total RNA-seq expression data on the same donors (Anthony Cutler, Arcadio Rubio Garcia and Chris Wallace), I found that 457 of the prioritised genes were expressed in at least one activation state. I could relate 259 genes to GWAS significant signals of which 166 were differentially expressed between activated and non activated states.

### 3.5 Comparison of COGS with TAD boundary prioritisation

### 3.6 Prioritised gene overlap with eQTLs

In parallel with my GWAS focused analysis Oliver Stegle and Roman Kretzhuber had been working to consider expression quantitative trait loci (eQTLs) from Fairfax et al [2012] in the context of PCHi-C. Both eQTL and GWAS are enriched in PIRs, which prompted us to consider the overlap of COGS prioritised genes in SLE [Bentham et al, 2015] and rheumatoid arthritis [Okada et al, 2014] data sets, for which full imputed summary statistics were available. we performed COGS gene prioritisation and looked to see if there was evidence for overlap with relevant tis-

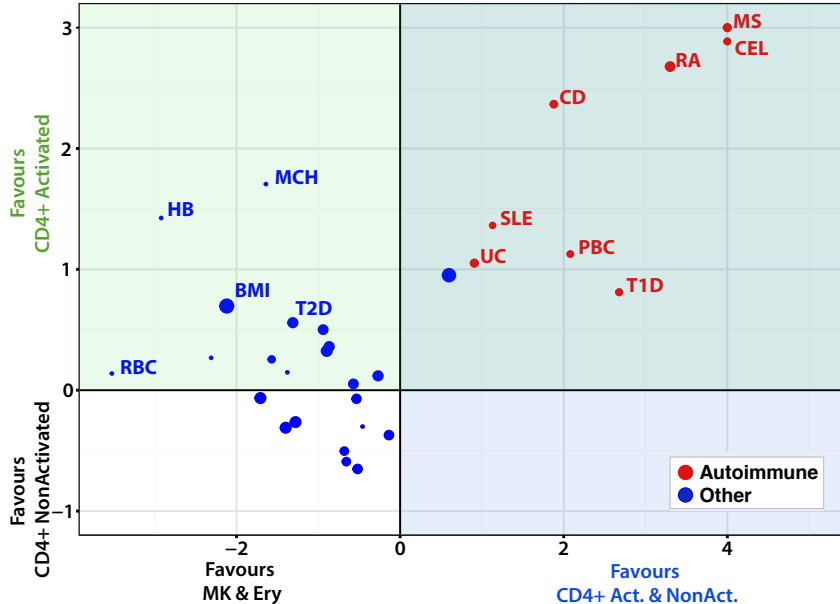


Figure 3.3: Tissue specific enrichment of autoimmune GWAS summary statistics at PIRs by tissue groups. Axes reflect *blockshifter* Z-scores for two different tissue group comparisons, firstly MK - megakaryocytes and ERY - erythroblast versus Activated/Non-activated CD4<sup>+</sup> T cells. Y-axis shows comparison of Activated versus non activated CD4<sup>+</sup> T cells. Autoimmune traits are coloured red and other traits are blue, point size reflects the log transformed sample number included in each study.

sue eQTLs [Fairfax et al, 2012]. Out of 456 genes that were prioritised for both traits 136 had eQTLs of which four genes (*BLK*, *RASGRP1*, *SUOX*, and *GIN1*) showed evidence for possible co-localization in RA and two genes (*BLK* and *SLC15A4*) in SLE. Additionally the genes prioritised for RA included 5/9 candidates (*C8Orf13*, *BLK*, *TRAF1*, *FADS2* and *SYNGR1*) that were identified in a recent study [Zhu et al, 2016] that combined whole blood eQTLs with the same RA GWAS data by Mendelian randomisation. The relatively large number of GWAS prioritised genes without eQTL support agrees with previous reports of limited overlap of disease variants with eQTLs [Guo et al, 2015; Huang et al, 2015b]. One reason for this observation might be that the causal variant functions in a specific tissue context and thus it's eQTL is not observable in available eQTL datasets. The implication of this is that regulatory annotations that might be used to augment fine mapping methods are similarly incomplete.

### 3.7 COGS prioritisation qualitatively performs better than TAD and distance based scores

For all eight GWAS autoimmune traits, I compared protein coding genes scores, using PCHiC datasets (COGS), and comparative scores computed using TAD and proximal methods. To summarise results across all diseases I selected the maximum score for a method for each gene. Using a score cut off of 0.5 I then categorised each gene as to whether it was prioritised in

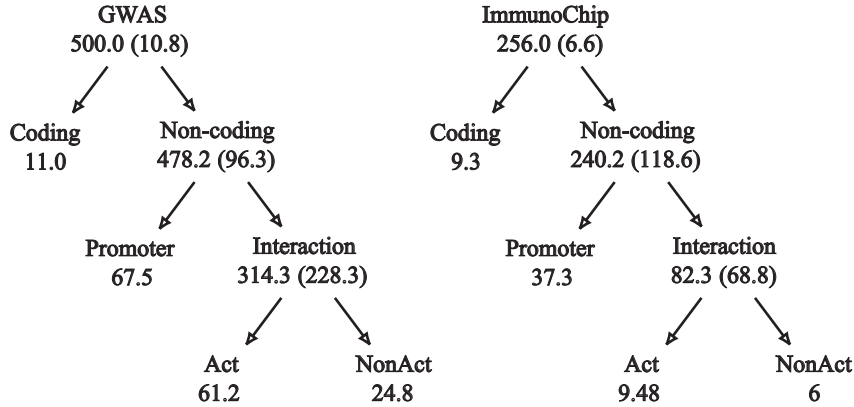


Figure 3.4: Functional gene prioritisation across 11 autoimmune diseases using genome wide (GWAS) or targeted genotyping array (ImmunoChip) data. The numbers at each node give the number of genes prioritised at that level. Where there is evidence to split into one of two non-overlapping hypotheses ( $\log_{10}$  ratio of gene scores  $>3$ ), the genes cascade down the tree. Where the evidence does not confidently predict which of the two possibilities is more likely, genes are ‘stuck’ at the parent node (number given in brackets). When the same gene is prioritised for multiple ( $n > 1$ ) disease, we assigned a fractional count to each node, defined as the proportion of the  $n$  disease for which the gene was prioritised at that node.

either a single, both or no methods (Figure ??). In general COGS prioritised genes sets were significantly smaller than those from the other methods. The naive proximity based score appeared to be least specific prioritising 5,731 genes in total, however it had the greatest overlap with COGS scores implying comparatively better sensitivity. For proximity based scores 83 genes were prioritised exclusively by COGS, indicating that 12% of genes are prioritised by interactions greater than 0.5 Mb. TAD based scores 219 genes were prioritised exclusively by COGS, indicating that approximately 30% of genes are prioritised by interactions that span TAD boundaries. I note however that examining distance metrics between gene baits and supporting PIRs that in some cases this could be due to the imprecise definition of TAD boundaries (Figure 3.7). Overall COGS appears to select genes not found by other methods and also appears to be more specific.

### 3.8 COGS prioritised genes are enriched for disease specific differentially expressed genes

Calibrating performance metrics of the COGS method is challenging in the absence of a test set of scores, one possible proxy is to examine the overlap of prioritised genes with studies examining differential expression between diseased and healthy volunteers in relevant tissue types. I integrated scores from PCHi-C (COGS), proximity and TAD methods, for ulcerative colitis (UC) and Crohn’s disease (CD), with differentially expressed genes (FDR 5%) from Peters et al [2016] and used Fishers Test to examine enrichment for prioritised genes (score  $> 0.5$ ). I found that UC COGS genes were significantly enriched for differentially expressed genes ( $P = 0.002$ ), for Crohn’s disease there was nominal enrichment ( $P = 0.04$ ). Conversely there was no

evidence of enrichment in any datasets using proximal and TAD methods (Figure 3.9). The intersect between differentially expressed genes and COGS prioritised genes identified 67 genes (Table 3). Whilst there are many candidate genes in this list, an example on chromosome 3 for ulcerative colitis provides an illustration of the potential for hypothesis generation by integrative analysis of PCHi-C interaction maps (Figure 3.8). COGS prioritises *BCL6* gene which has been shown to have potent effects on Th9 cell development and IL-9 secretion both important modulators of inflammation [?]. Putative causal variants from Anderson et al [2011] reside in intron 8 of *LPP*, and previous studies have inferred this gene as responsible for, however PCHi-C results from lymphoid tissues show interactions between this region and the *BCL6* promoter. Furthermore, BLUEPRINT chromatin state maps classify this region harbouring putative causal variants as having enhancer activity across 3 out of 4 biological replicates in CD4<sup>+</sup> T cells. Expression profiles from Peters et al [2016] show that whilst *LPP* is not significantly differentially expressed between UC controls and healthy volunteers( $\log(\text{Fold Change}) = 0.05$ ,  $P_{adj} = 0.46$ ) *BCL6* ( $\log(\text{Fold Change}) = 0.22$ ,  $P_{adj} = 0.0018$ ), providing further support for it's prioritisation.

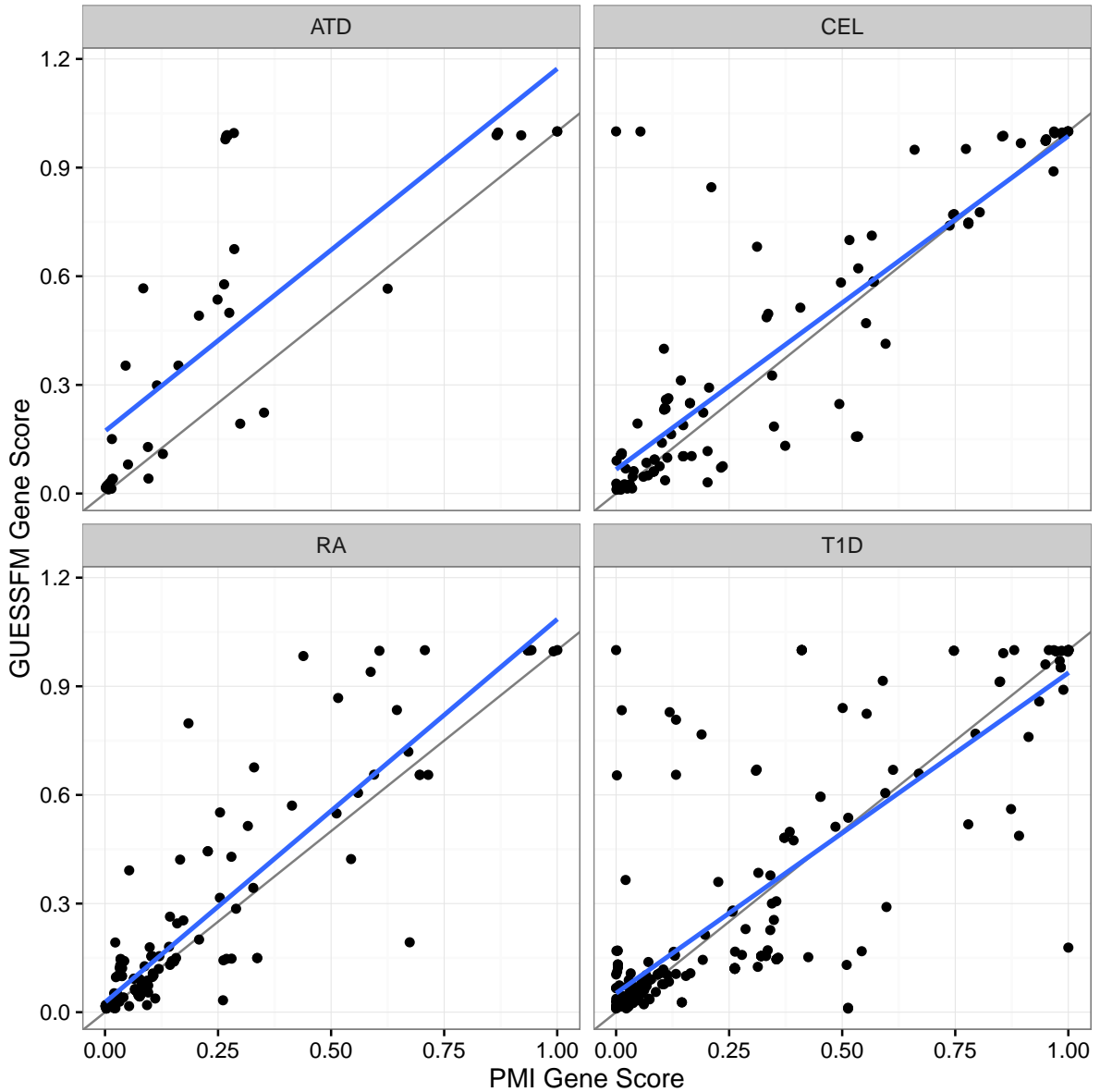


Figure 3.5: Comparison of COGS gene scores for four autoimmune traits (ATD = autoimmune thyroid disease, CEL = celiac disease, RA = rheumatoid arthritis and T1D = type 1 diabetes computed using marginal posteriors from GUESSFM method and those computed using posteriors from PMI, grey line shows  $y = x$ , blue lines indicate the fitting of a linear model

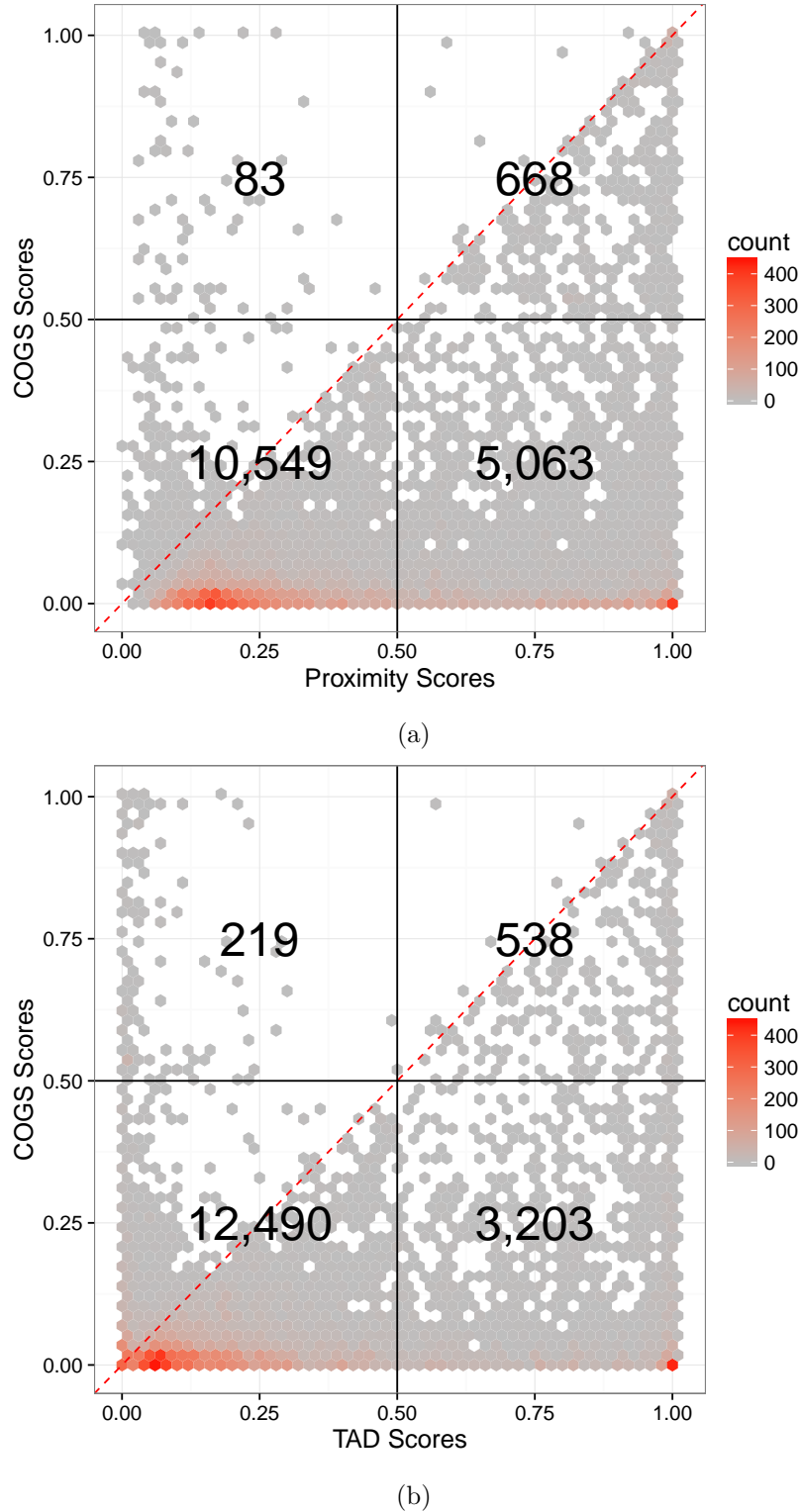


Figure 3.6: Comparison of autoimmune PCHi-C COGS scores and (a) a proximity score from assigning variants to genes within 0.5 Mb of gene promoters (b) Hi-C derived TAD scores, using 7 Cell types (Erythroblasts, Macrophages, Monocytes, Naive B cells, Naive CD4<sup>+</sup> T cells, Naive CD8<sup>+</sup> T cells and Neutrophils). Counts of genes in each quadrant are shown, grey to red colour gradient indicates gene density.

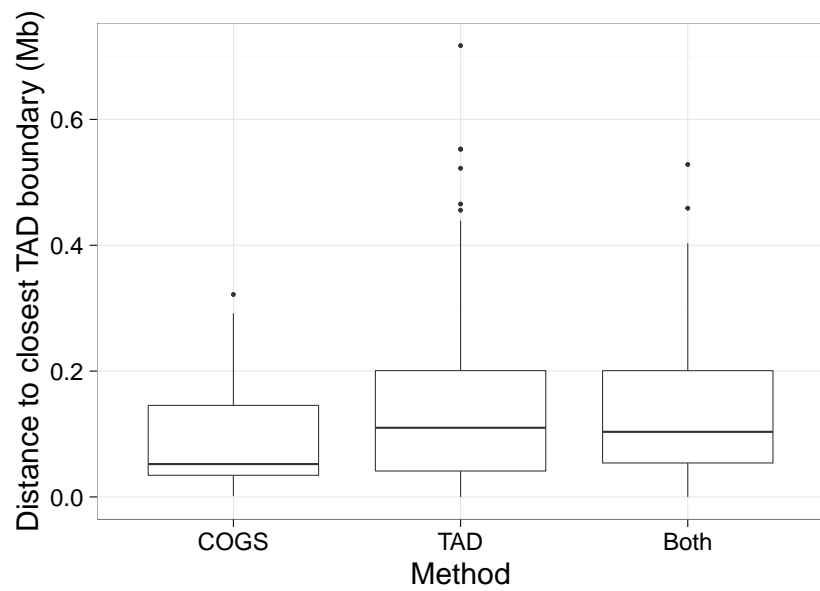


Figure 3.7: Box plot showing the distribution of distances between baits and TAD boundaries for significant (score > 0.5) genes. Both indicates that gene was significant using TAD and COGS methods

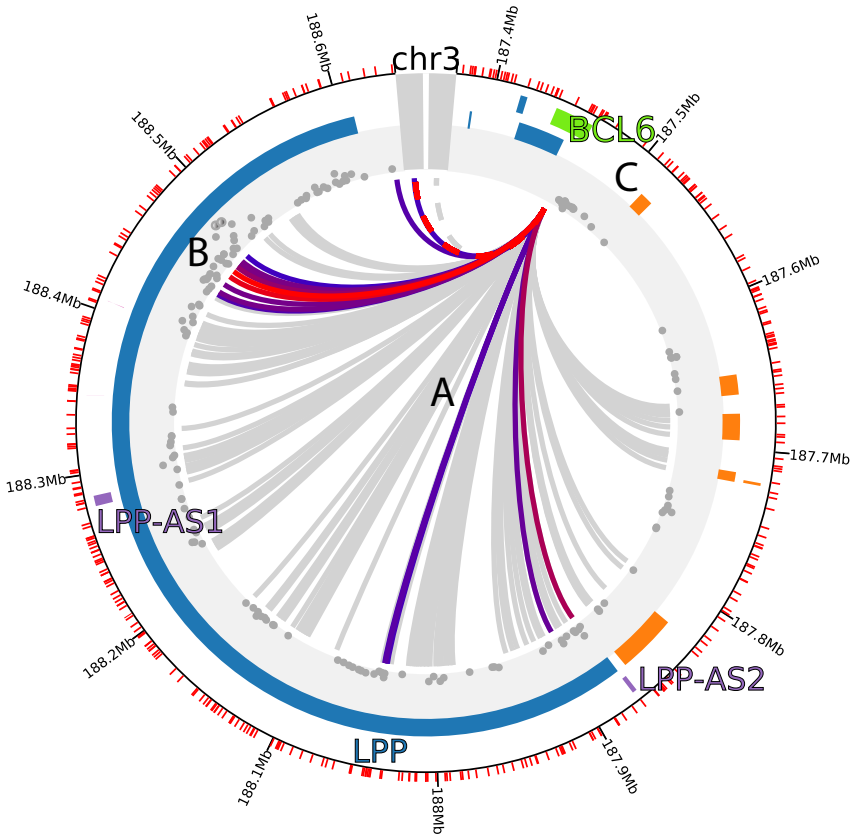


Figure 3.8: Circularised plot showing overlap between ulcerative colitis (UC) putative variants and interactions between *BCL6* gene promoter in CD4<sup>+</sup> T cells, prioritised by COGS algorithm. A) Interactions, grey (not significant (CHiCAGO score < 5 but significant in other tissues), blue (less significant) to red(more significant) colour gradient. B) UC GWAS summary – log( $P$ ) values from Anderson et al [2011] C) Gene annotations, protein coding (blue), anti-sense (purple), lincRNA (orange) and *BCL6* (green). Red ticks around circumference indicate *HindIII* fragment boundaries. Figure modified from CHiCP <http://www.chicp.org> [Schofield et al, 2016]

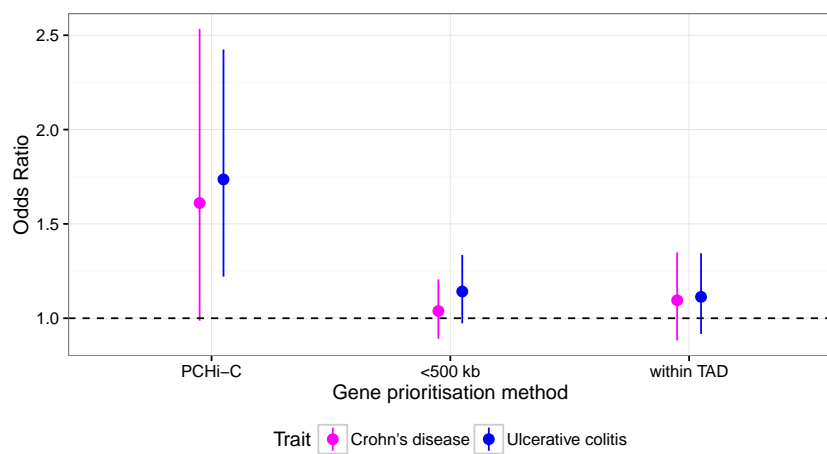


Figure 3.9: Enrichment of prioritised genes in ulcerative colitis and Crohn's differentially expressed genes from Peters et al [2016]. Methods PCHi-C (COGS), < 500 Kb (Proximity) and within TAD (topologically associated domain).

# Chapter 4

## Discussion

### 4.1 Functional validation of COGS prioritised gene *IL2RA*

COGS analysis prioritised, in multiple diseases (autoimmune thyroid disease, Crohn's disease, multiple sclerosis, rheumatoid arthritis, type 1 diabetes, and ulcerative colitis) *IL2RA* which encodes the CD25 protein which is a component of the IL-2 receptor that is essential for high-affinity binding of IL-2, regulatory T cell survival and T effector cell differentiation and function(add references). I found this prioritisation to be driven by an interaction between the *IL2RA* promoter and a PIR in exon 1 known to harbour a set of type 1 diabetes putative causal SNPs (Figure??) identified in a previous fine mapping study [Wallace et al, 2015]. This 'A' set of SNPs(Figure??a) is in high LD ( $r^2 > 0.8$ ) with rs12722495 which has been shown to affect the surface expression CD25 in memory T cells [Dendrou et al, 2009]. Using a targeted RNA-sequencing approach, and using software I developed previously [Rainbow et al, 2015] we measured the relative expression of the two alleles at one of these set 'A' SNPs, rs61839660, in intronic cDNA from four individuals heterozygous at rs61839660 and homozygous across most other associated SNP groups, in a four-hour activation time-course of CD4+ T cells. We observed allelic imbalance in non activated CD4+ T cells however on activation this was lost suggesting a context specific effect within this locus. This was further validated using rs12244380 found in the 3' UTR of *IL2RA* (Figure4.2).

### 4.2 Limitations

There are a number of limitations with the current approaches that I have developed. Firstly the fine mapping approach employed assumes for a given region a simplified model of a single underlying causal variant. This clearly effects the output of the COGS algorithm (figure 3.5) where I compare COGS scores for genes using PMI approach and using GUESSFM which considers any number of causal variants. Whilst there is no "gold standard" in COGS gene scores to compare, in general GUESSFM seems to prioritise more genes than PMI (Table ??). A portion of this might be better the resolution that the GUESSFM approach favours, however some of this will be offset by it's sensitivity to genotyping error.

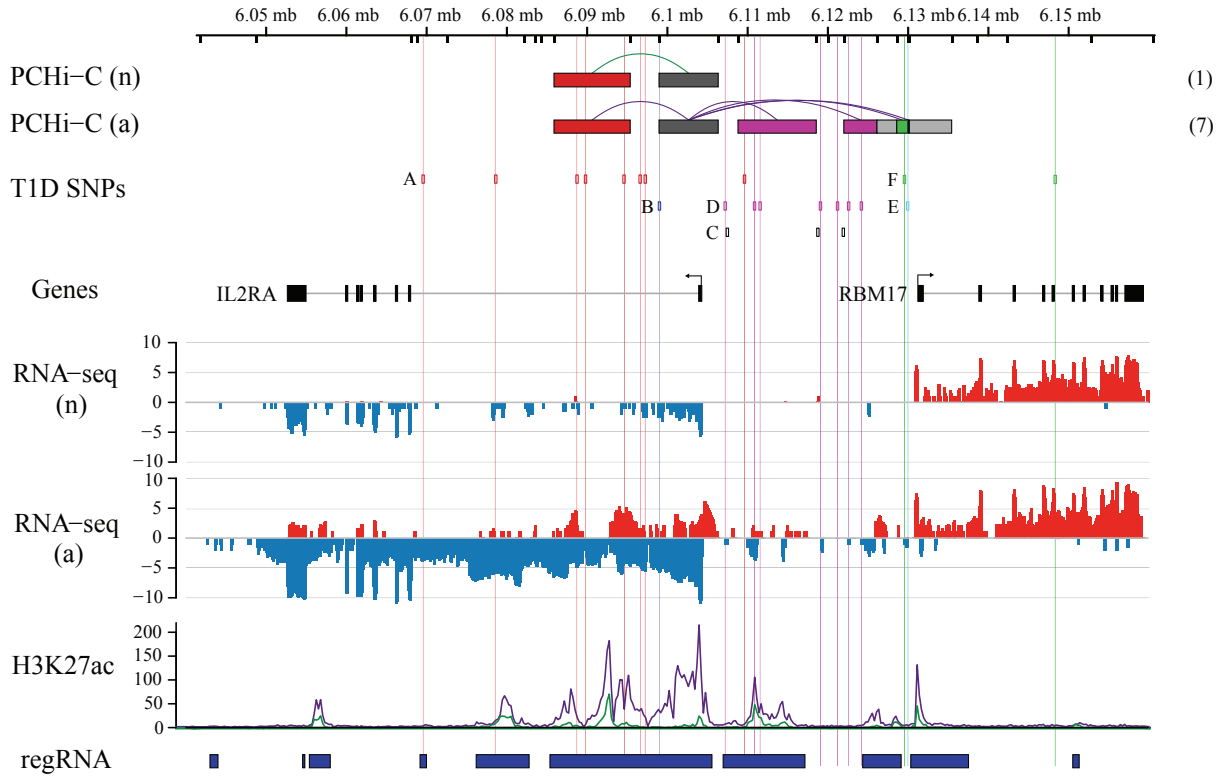


Figure 4.1: PCHi-C interactions link the *IL2RA* promoter to autoimmune disease associated genetic variation which leads to expression differences in *IL2RA* mRNA.

Disease	GUESSFM	PMI	Both	Total
ATD	9	0	6	38
CEL	6	5	33	114
RA	6	2	19	132
T1D	16	7	35	212

Table 4.1: Counts for protein coding genes prioritised (score > 0.5) by GUESSFM, Poor Man's Imputation (PMI) and Both methods out of Total genes with score > 0.01.

Another limitation is the thresholded approach to CHiCAGO scores that are used to call interactions, all of the methods developed so far use a threshold score of 5, in practice an interaction with a score of 4.99 will be omitted. Future approaches might investigate methods for incorporating promoter interaction scores in both *blockshifter* and COGS methods. One approach might be to look at techniques that utilise CHiCAGO scores across multiple tissues for a given interaction to adjust local FDR.

COGS assumes that coding variation effects gene within which it is located, however studies in model organisms [Lawrie et al, 2013] and in humans [Stergachis et al, 2013] indicate that coding variation can fulfil a dual role in the regulation of genes. With this in mind, questions include whether such variation has a *cis* effect on other genes by functioning as regulatory DNA as well as whether we can improve the granularity of coding variant hypothesis by further subdivision (e.g. non-synonymous and synonymous).

One significant problem with these analysis is that resolution is limited by *Hind*III restriction fragment length. This manifests in two main ways, firstly there is a blind spot for observing shorter range interactions that involve *Hind*III adjoining baited interactions. I have attempted to capture these as ‘promoter’ regions (Figure 2.2) however integration with functional annotation might provide further resolution and identify functional hypothesis for mechanisms for further study. The second more pernicious issue is that many baited fragments are promiscuous in that they contain promoter regions for more than one gene. If we consider just protein coding genes then of 16,608 baits 3,009 (18%) contain multiple promoters from different genes, if we include all transcriptional start site annotations in Ensembl (Version 75) then this rises to 6,703 (40%), in reality this is a conservative estimate due to the incomplete annotation of the non-coding genome. For these promiscuous baits it is impossible to resolve which promoter or promoters are involved in the chromatin looping, using PCHI-C data alone, one possible naive solution is to integrate context specific expression data to match genes expressed in that context to possible context specific interactions. This leads on to another possible extension which is to extend prioritisation to include annotated non coding genes as a recent study suggests that these modulate autoimmune disease susceptibility [Castellanos-Rubio et al, 2016].

Excluding single cell implementations all genomic technologies give an overview of the molecular events across the range of cells being assayed. In the case of immune subsets this is particularly relevant as broad categories, such as CD4+ T cells will be heterogeneous containing further subdivisions that may or may not be relevant for disease biology. It is important to bear this in mind when considering PCHI-C maps as without single cell profiling it is impossible to resolve whether interactions are common across the assayed tissue type or are specific to an underlying and as yet unsorted subset.

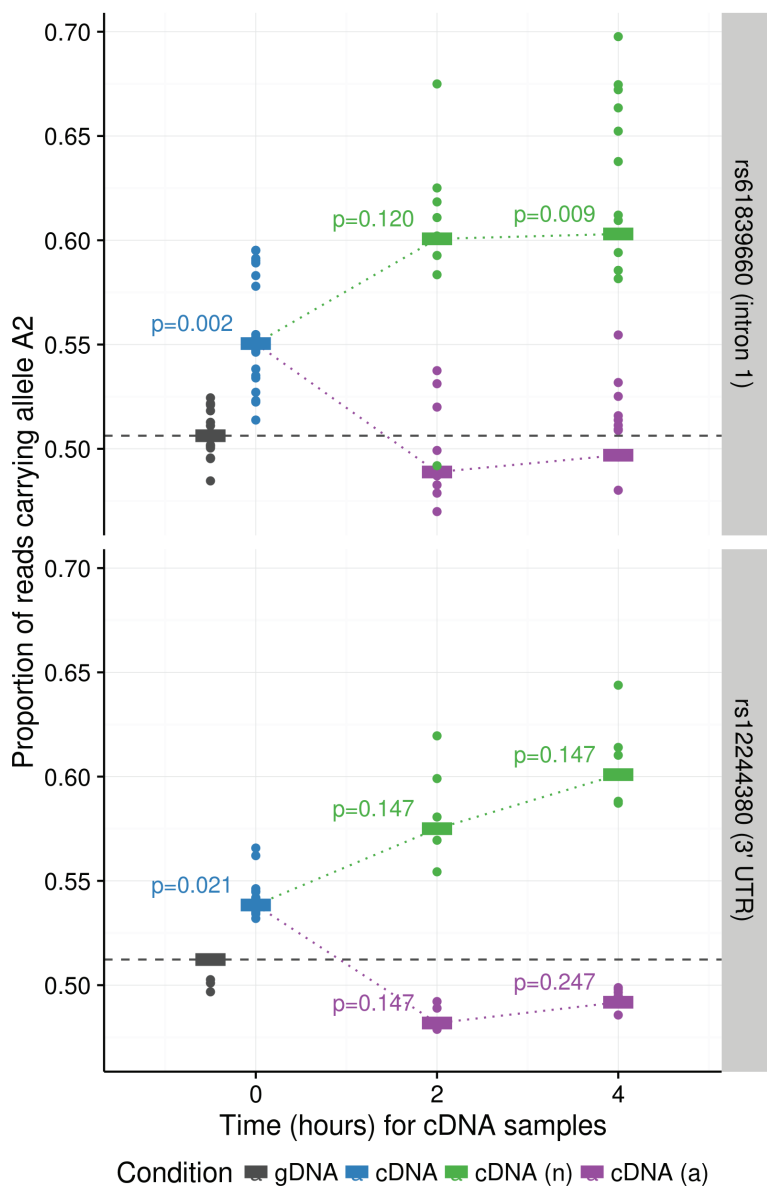


Figure 4.2: *=IL2RA* ASE data - needs caption.

# Chapter 5

## Future Work

### 5.1 Application of COGS scores to the full PCHiC dataset

Having shown evidence that the COGS tissue specific prioritisation score is useful, I have begun the process of applying it across all traits to all 17 tissue types. For each trait it should be possible to generate a decision tree as in Figure 5.1. If this is successful I would like to examine metrics for comparing tree structures and therefore inter trait relationships (Figure ??).

### 5.2 Comparison with Hi-C defined TAD boundaries

So far it is unclear as to how much information is gained in gene prioritisation using promoter capture Hi-C over classical Hi-C. Csilla Varnai and Michiel Thiecke have generated TAD domain boundaries for 8 of the 17 cell types assayed using conventional Hi-C libraries. I will use these to generate pseudo interaction matrices whereby within each TAD the promoter of all genes interacts with every fragment, excepting the baited fragment, and those bounding it for a given gene within a TAD. For these tissues for which Hi-C libraries are available I will also compute gene scores using COGS and analyse the differences to see whether information is gained from using promoter-capture Hi-C over classical Hi-C.

### 5.3 Integrating other annotations into COGS

PMI assumes a fixed prior for all SNPs however recent work [Pickrell, 2014] using Bayesian hierarchical frameworks demonstrates a method by which we can estimate variable priors for each SNP based on other sources of annotation. In the hierarchical method implemented by *fgwas* for a given SNP the prior probability for association,  $\pi_{ik}$ , varies depending on the enrichment of annotations,  $\lambda_l$ .

$$\pi_{ik} = \frac{e^{x_i}}{\sum_{j \in S_k} e^{x_j}} \quad (5.1)$$

$x_i$  is the sum of the effect of all the annotations that the  $i^{th}$  SNP overlaps as shown below.

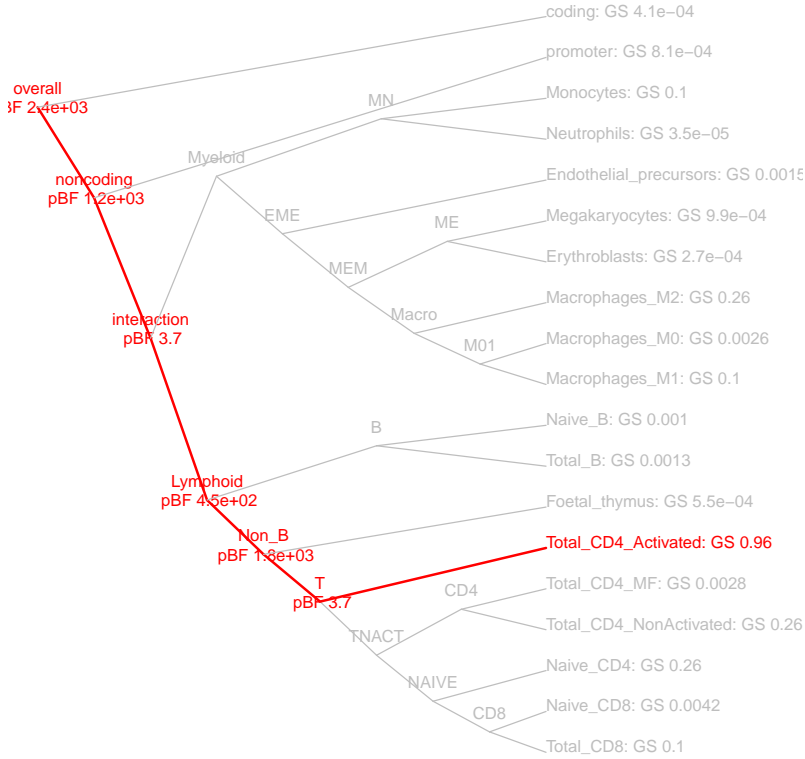


Figure 5.1: COGS decision dendrogram using rheumatoid arthritis data from Okada et al and PCHi-C maps from 17 haematopoietic cell types for the *AHR* gene. The red edges denote the path taken by COGS through the binary decision tree. Each node is labelled with pseudo Bayes factors(pBF). Terminal nodes are labelled with the tissue/annotation specific gene score(GS)

Here  $\lambda_l$  is the effect of annotation  $l$  and  $I_{il}$  is an indicator function as to whether SNP  $i$  overlaps annotation  $l$ .

$$x_i = \sum_{l=1}^{L_2} \lambda_l I_{il} \quad (5.2)$$

Initially I would use further information on  $CD4^+$  T cells including various histone-modification marks and methylation data alongside publicly available annotations to compute  $\lambda_l$  using *fg-was*. Using a model including the most relevant annotations these  $x_i$  values could also be applied to compute variable priors ( $\pi_i$ ) for dense ImmunoChip summary statistics. These more annotation aware posterior probabilities will then be input into COGS to see how this alters gene prioritisation. If this was successful I would look into the incorporation of other BLUEPRINT annotations across all 31 traits.

## 5.4 blockshifter development - perhaps omit

Demonstrating the enrichment of an annotation for associated variants robustly in the presence of correlation is challenging. Correlation, occurring through linkage disequilibrium between SNPs and between genomic annotations, has the effect of inflating the underlying test statistic and must be carefully adjusted for. The *blockshifter* approach does this using a mixture of circularised and weighted permutation techniques using underlying *HindIII* fragments as atomic units to define underlying block structure. I will investigate the utility of *blockshifter* outside of the PCHiC initially looking at it's performance using (un)activated CD4<sup>+</sup> T cell ChIP-Seq data sets. In this case I am not limited to *HindIII* but will assay the performance of more frequent cutters (e.g. *SspI*) in terms of results and computational efficiency.

## 5.5 Tissue specific gene set enrichment analysis

TODO

## 5.6 Data driven discovery of relevant COGS score thresholds

TODO

## 5.7 Future Directions

In the longer term I hope to collaborate with clinicians to build promoter capture Hi-C maps of relevant tissues in disease and healthy states. Controlling for variation between individuals in this context is paramount, thus employing strategies to overcome this within the bounds of the economic and technical limitations is important. One strategy is to compare diseased and healthy tissue within the same individual, taken at the same time point to look for differences in interactions, an example of this might be in juvenile idiopathic arthritis (JIA), here the diseased tissue is known and samples, in the form of synovial fluid drains for are available. PCHi-C results generated from CD4+ T cells isolated from the same individual might be compared with those isolated from the periphery. Another complimentary strategy for systemic autoimmune disease where diseased tissue is challenging to collect is to take a longitudinal approach, here patients presenting with a disease are assayed, with further follow up assays collected over time taking into account any therapeutic interventions. Genomic comparison between time points is then conducted to look for differential interactions that might be related to disease prognosis. Further evidence of for a genes involvement in autoimmune disease susceptibility might come from adapting the methods previously described to work with rare variants. For this work one could use gene level variant aggregation tests [Lee et al, 2013] and then use genotype data from primary immune disorders collected as part of the BRIDGE study, PCHiC data would be used to assign variants to genes allowing the integration of both coding and non-coding variation.

Table 1: Summary of PCHi-C datasets generated in this study

Cell type	Acronym	Biological replicates	Unique captured read pairs	Detected interactions
Megakaryocytes	MK	4	653,848,788	150,203
Erythroblasts	Ery	3	588,786,672	144,771
Neutrophils	Neu	3	736,055,569	131,609
Monocytes	Mon	3	572,357,387	151,389
Macrophages M0	M $\phi$ 0	3	668,675,248	163,791
Macrophages M1	M $\phi$ 1	3	497,683,496	163,399
Macrophages M2	M $\phi$ 2	3	523,561,551	173,449
Endothelial Precursors	EndP	3	420,536,621	141,382
Naive B cells	nB	3	629,928,642	171,439
Total B cells	tB	3	702,533,922	183,119
Fetal Thymus	FetT	3	776,491,344	145,577
Naive CD4+ T cells	nCD4	4	844,697,853	192,048
Total CD4+ T cells	tCD4	3	836,974,777	166,668
Non-Activated Total CD4+ T cells	naCD4	3	721,030,702	177,371
Activated Total CD4+ T cells	aCD4	3	749,720,649	188,714
Naive CD8+ T cells	nCD8	3	747,834,572	187,399
Total CD8+ T cells	tCD8	3	628,771,947	183,964
Total			11,299,489,740	708,007 <sup>1</sup>

<sup>1</sup>Unique interactions captured in at least one cell type

Table 2: Summary of GWAS summary statistics used in this study

Trait	Acronym	Cases	Controls	Study Type	PMID	First Author(Date)	# SNPs	Source
Platelet volume	PV	18600		QUANT	22139419	Gieger(2011)	2231438	N Soranzo personal communication
Platelet count	PLT	48666		QUANT	22139419	Gieger(2011)	2206665	N Soranzo personal communication
Mean corpuscular volume	MCV	4627		QUANT	19820697	Soranzo(2009)	2156669	N Soranzo personal communication
Packed cell volume	PCV	4627		QUANT	19820697	Soranzo(2009)	2009357	N Soranzo personal communication
Red blood cell count	RBC	4627		QUANT	19820697	Soranzo(2009)	2091590	N Soranzo personal communication
Haemoglobin	HB	4627		QUANT	19820697	Soranzo(2009)	1640923	N Soranzo personal communication
Mean corpuscular haemoglobin	MCH	4627		QUANT	19820697	Soranzo(2009)	1904974	N Soranzo personal communication
Mean corpuscular haemoglobin concentration	MCHC	4627		QUANT	19820697	Soranzo(2009)	2070334	N Soranzo personal communication
Ulcerative colitis Anderson	UC	6687	19718	CC	21297633	Ander-son(2011)	1399283	<a href="http://www.immunobase.org">http://www.immunobase.org</a>
Multiple sclerosis IMSGC	MS	9772	17376	CC	21833088	IMSGC(2011)	463628	<a href="http://www.immunobase.org">http://www.immunobase.org</a>
Type 1 diabetes Barrett	T1D	8000	8000	CC	19430480	Barrett(2009)	789849	<a href="http://www.immunobase.org">http://www.immunobase.org</a>

Continued on next page

Trait	Acronym	Cases	Controls	Study Type	PMID	First Author(Date)	# SNPs	Source
Celiac disease DuBois	CEL	4533	10750	CC	20190752	Dubois(2010)	509768	<a href="http://www.immunobase.org">http://www.immunobase.org</a>
Crohn's disease immunobase	CD	6333	15056	CC	21102463	Franke(2010)	950208	<a href="http://www.immunobase.org">http://www.immunobase.org</a>
Rheumatoid arthritis Okada	RA	14361	43923	CC	24390342	Okada(2014)	8513749	<a href="http://plaza.umin.ac.jp/~okada/datasource/files/GWASMetaResults/RA_GWASmeta_European_v2.txt.gz">http://plaza.umin.ac.jp/~okada/datasource/files/GWASMetaResults/RA_GWASmeta_European_v2.txt.gz</a>
Type 2 diabetes	T2D	12171	56860	CC	22885922	Morris(2012)	2075585	<a href="http://diagram-consortium.org/downloads.html">http://diagram-consortium.org/downloads.html</a>
Height	HT	253288		QUANT	25282103	Wood(2014)	1927160	<a href="https://www.broadinstitute.org/collaboration/giant/images/0/01/GIANT_HEIGHT_Wood_et_al_2014_publicrelease_HapMapCeuFreq.txt.gz">https://www.broadinstitute.org/collaboration/giant/images/0/01/GIANT_HEIGHT_Wood_et_al_2014_publicrelease_HapMapCeuFreq.txt.gz</a>

Continued on next page

Trait	Acronym	Cases	Controls	Study Type	PMID	First Author(Date)	# SNPs	Source
Tryglycerides	TG	96598		QUANT	20686565	Teslovich(2010)	2304026	<a href="http://csg.sph.umich.edu/abecasis/public/lipids2010/TG2010.zip">http://csg.sph.umich.edu/abecasis/public/lipids2010/TG2010.zip</a>
High density lipoprotein	HDL	99900		QUANT	20686565	Teslovich(2010)	2322449	<a href="http://csg.sph.umich.edu/abecasis/public/lipids2010/HDL2010.zip">http://csg.sph.umich.edu/abecasis/public/lipids2010/HDL2010.zip</a>
Low density lipoprotein	LDL	95454		QUANT	20686565	Teslovich(2010)	2298548	<a href="http://csg.sph.umich.edu/abecasis/public/lipids2010/LDL2010.zip">http://csg.sph.umich.edu/abecasis/public/lipids2010/LDL2010.zip</a>
Total Cholesterol	TC	100184		QUANT	20686565	Teslovich(2010)	2323152	<a href="http://csg.sph.umich.edu/abecasis/public/lipids2010/TC2010.zip">http://csg.sph.umich.edu/abecasis/public/lipids2010/TC2010.zip</a>
Glucose sensitivity BMI adjusted	GLC_B	58074		QUANT	22581228	Manning(2012)	2622994	<a href="ftp://ftp.sanger.ac.uk/pub/magic/MAGIC_Manning_et_al_FastingGlucose_MainEffect.txt.gz">ftp://ftp.sanger.ac.uk/pub/magic/MAGIC_Manning_et_al_FastingGlucose_MainEffect.txt.gz</a>

Continued on next page

Trait	Acronym	Cases	Controls	Study Type	PMID	First Author(Date)	# SNPs	Source
Glucose sensitivity	GLC	58074		QUANT	22581228	Manning(2012)	2622996	<a href="ftp://ftp.sanger.ac.uk/pub/magic/MAGIC_Manning_et_al_FastingGlucose_MainEffect.txt.gz">ftp://ftp.sanger.ac.uk/pub/magic/MAGIC_Manning_et_al_FastingGlucose_MainEffect.txt.gz</a>
Insulin sensitivity BMI adjusted	INS_B	51750		QUANT	22581228	Manning(2012)	2621974	<a href="ftp://ftp.sanger.ac.uk/pub/magic/MAGIC_Manning_et_al_lnFastingInsulin_MainEffect.txt.gz">ftp://ftp.sanger.ac.uk/pub/magic/MAGIC_Manning_et_al_lnFastingInsulin_MainEffect.txt.gz</a>
Insulin sensitivity	INS	51750		QUANT	22581228	Manning(2012)	2621977	<a href="ftp://ftp.sanger.ac.uk/pub/magic/MAGIC_Manning_et_al_lnFastingInsulin_MainEffect.txt.gz">ftp://ftp.sanger.ac.uk/pub/magic/MAGIC_Manning_et_al_lnFastingInsulin_MainEffect.txt.gz</a>
Femoral neck bone mineral density	FNBMD	32961		QUANT	22504420	Estrada(2012)	2473840	<a href="http://www.gefoss.org/sites/default/files/GEFOS2_FNBMD_POOLED_GC.txt.gz">http://www.gefoss.org/sites/default/files/GEFOS2_FNBMD_POOLED_GC.txt.gz</a>

Continued on next page

Trait	Acronym	Cases	Controls	Study Type	PMID	First Author(Date)	# SNPs	Source
Lumbar spine bone mineral density	LS-BMD	32961		QUANT	22504420	Estrada(2012)	2463611	<a href="http://www.gefoss.org/sites/default/files/GEFOS2 LSBMD POOLED_GC.txt.gz">http://www.gefoss.org/sites/default/files/GEFOS2 LSBMD POOLED_GC.txt.gz</a>
Diastolic blood pressure	BP_D	69395		QUANT	21909115	ICBP(2011)	2460847	<a href="http://www.georgehretlab.org/ICBP-summary-Nature.csv.gz">http://www.georgehretlab.org/ICBP-summary-Nature.csv.gz</a>
Systolic blood pressure	BP_S	69395		QUANT	21909115	ICBP(2011)	2460847	<a href="http://www.georgehretlab.org/ICBP-summary-Nature.csv.gz">http://www.georgehretlab.org/ICBP-summary-Nature.csv.gz</a>
Body Mass Index	BMI	322200		QUANT	25673413	Locke(2015)	1984096	<a href="https://www.broadinstitute.org/collaboration/giant/images/1/15/SNP_gwas_mc_merge_nogc.tbl.uniq.gz">https://www.broadinstitute.org/collaboration/giant/images/1/15/SNP_gwas_mc_merge_nogc.tbl.uniq.gz</a>
Systemic Lupus Erythrematosis	SLE	4036	6959	CC	26502338	Ben-tham(2015)	7734064	<a href="http://www.immunobase.org">http://www.immunobase.org</a>
Primary Billiary Cirrhosis	PBC	2764	10475	CC	26394269	Cordell(2015)	1134133	<a href="http://www.immunobase.org">http://www.immunobase.org</a>

Table 3: Summary of GWAS summary statistics used in this study

Gene Name	COGS score	DE $P_{adj}$	Disease
FAIM3	1.000	0.000	UC
COX4I1	1.000	0.036	UC
RPS24	1.000	0.011	CD
IKZF1	0.999	0.001	CD
ACSS1	0.999	0.017	UC
CHD1	0.988	0.032	CD
CD274	0.987	0.002	CD
ROPN1L	0.944	0.042	UC
ADO	0.941	0.006	CD
TFAM	0.939	0.001	CD
ETS1	0.934	0.001	UC
MIDN	0.927	0.011	CD
SBNO2	0.926	0.000	CD
IPMK	0.922	0.028	CD
RQCD1	0.914	0.038	UC
STK32B	0.894	0.022	UC
CTDSP1	0.877	0.008	UC
ADAM10	0.854	0.006	UC
MYC	0.836	0.034	CD
FCGR2A	0.836	0.021	UC
FCRLA	0.835	0.018	UC
SGMS1	0.835	0.000	UC
CD244	0.823	0.003	CD
PIM3	0.822	0.001	UC
BCL6	0.811	0.001	UC
RTP2	0.800	0.043	UC
RASGRP1	0.795	0.005	CD
IKZF3	0.793	0.000	UC
LYRM7	0.771	0.001	UC
DGKD	0.758	0.004	CD
CHRNE	0.737	0.041	UC
ARRB2	0.717	0.001	UC
PIP4K2C	0.686	0.009	UC
ADAM9	0.684	0.000	UC
Continued on next page			

Gene Name	COGS score	DE P <sub>adj</sub>	Disease
GATA3	0.679	0.031	UC
PAPD7	0.659	0.007	UC
MFF	0.658	0.020	UC
IGF2	0.649	0.049	UC
STK36	0.634	0.013	UC
GPX4	0.631	0.000	CD
BEST1	0.627	0.001	CD
ATG4D	0.626	0.017	CD
AGAP2	0.621	0.017	UC
SMAD3	0.612	0.013	CD
MRPL4	0.599	0.017	CD
MARCH9	0.594	0.003	UC
MAN2A2	0.591	0.038	CD
GALC	0.589	0.001	CD
CDK4	0.588	0.014	UC
MLC1	0.575	0.031	CD
DSE	0.573	0.000	UC
BCL2	0.565	0.015	UC
FBL	0.561	0.001	UC
C9orf37	0.543	0.001	UC
DPP7	0.542	0.047	UC
SSNA1	0.542	0.000	UC
PHPT1	0.542	0.007	UC
CCDC183	0.542	0.012	UC
ABCA2	0.542	0.021	UC
SCAMP3	0.529	0.020	CD
TTC1	0.523	0.045	UC
ZBTB49	0.520	0.047	UC
CD55	0.517	0.002	UC
FYB	0.508	0.008	CD
ATF6	0.504	0.003	UC

# Bibliography

- Albert FW and Kruglyak L. 2015. The role of regulatory variation in complex traits and disease. *Nat. Rev. Genet.* **16**: 197–212.
- Anderson CA, Boucher G, Lees CW, Franke A, D'Amato M, Taylor KD, Lee JC, Goyette P, Imielinski M, Latiano A, et al. 2011. Meta-analysis identifies 29 additional ulcerative colitis risk loci, increasing the number of confirmed associations to 47. *Nat. Genet.* **43**: 246–252.
- Bentham J, Morris DL, Cunningham Graham DS, Pinder CL, Tombleson P, Behrens TW, Martín J, Fairfax BP, Knight JC, Chen L, et al. 2015. Genetic association analyses implicate aberrant regulation of innate and adaptive immunity genes in the pathogenesis of systemic lupus erythematosus. *Nat. Genet.* .
- Burren OS, Guo H, and Wallace C. 2014. VSEAMS: a pipeline for variant set enrichment analysis using summary GWAS data identifies IKZF3, BATF and ESRRA as key transcription factors in type 1 diabetes. *Bioinformatics* **30**: 3342–3348.
- Cairns J, Freire-Pritchett P, Wingett SW, Várnai C, Dimond A, Plagnol V, Zerbino D, Schoenfelder S, Javierre BM, Osborne C, et al. 2016. Chicago: robust detection of dna looping interactions in capture hi-c data. *Genome Biol* **17**: 127.
- Castellanos-Rubio A, Fernandez-Jimenez N, Kratchmarov R, Luo X, Bhagat G, Green PHR, Schneider R, Kiledjian M, Bilbao JR, and Ghosh S. 2016. A long noncoding rna associated with susceptibility to celiac disease. *Science* **352**: 91–95.
- Claussnitzer M, Dankel SN, Kim KH, Quon G, Meuleman W, Haugen C, Glunk V, Sousa IS, Beaudry JL, Puviindran V, et al. 2015. Fto obesity variant circuitry and adipocyte browning in humans. *N Engl J Med* **373**: 895–907.
- Cooper GS, Bynum MLK, and Somers EC. 2009. Recent insights in the epidemiology of autoimmune diseases: improved prevalence estimates and understanding of clustering of diseases. *J Autoimmun* **33**: 197–207.
- Cortes A and Brown MA. 2011. Promise and pitfalls of the immunochip. *Arthritis Res Ther* **13**: 101.

- Davison LJ, Wallace C, Cooper JD, Cope NF, Wilson NK, Smyth DJ, Howson JMM, Saleh N, Al-Jeffery A, Angus KL, et al. 2012. Long-range DNA looping and gene expression analyses identify DEXI as an autoimmune disease candidate gene. *Hum. Mol. Genet.* **21**: 322–333.
- Dendrou CA, Plagnol V, Fung E, Yang JHM, Downes K, Cooper JD, Nutland S, Coleman G, Himsworth M, Hardy M, et al. 2009. Cell-specific protein phenotypes for the autoimmune locus il2ra using a genotype-selectable human bioresource. *Nat Genet* **41**: 1011–1015.
- Fabregat A, Sidiropoulos K, Garapati P, Gillespie M, Hausmann K, Haw R, Jassal B, Jupe S, Korninger F, McKay S, et al. 2016. The reactome pathway knowledgebase. *Nucleic Acids Res* **44**: D481–D487.
- Fairfax BP, Makino S, Radhakrishnan J, Plant K, Leslie S, Dilthey A, Ellis P, Langford C, Vannberg FO, and Knight JC. 2012. Genetics of gene expression in primary immune cells identifies cell type-specific master regulators and roles of hla alleles. *Nat Genet* **44**: 502–510.
- Farh KKH, Marson A, Zhu J, Kleinewietfeld M, Housley WJ, Beik S, Shores N, Whitton H, Ryan RJ, Shishkin AA, et al. 2015. Genetic and epigenetic fine mapping of causal autoimmune disease variants. *Nature* **518**: 337–343.
- Franke A, McGovern DPB, Barrett JC, Wang K, Radford-Smith GL, Ahmad T, Lees CW, Balschun T, Lee J, Roberts R, et al. 2010. Genome-wide meta-analysis increases to 71 the number of confirmed crohn's disease susceptibility loci. *Nat. Genet.* **42**: 1118–1125.
- Fullwood MJ, Liu MH, Pan YF, Liu J, Xu H, Mohamed YB, Orlov YL, Velkov S, Ho A, Mei PH, et al. 2009. An oestrogen-receptor-alpha-bound human chromatin interactome. *Nature* **462**: 58–64.
- Giambartolomei C, Vukcevic D, Schadt EE, Franke L, Hingorani AD, Wallace C, and Plagnol V. 2014. Bayesian test for colocalisation between pairs of genetic association studies using summary statistics. *PLoS Genet* **10**: e1004383.
- Guo H, Fortune MD, Burren OS, Schofield E, Todd JA, and Wallace C. 2015. Integration of disease association and eQTL data using a bayesian colocalisation approach highlights six candidate causal genes in immune-mediated diseases. *Hum. Mol. Genet.* .
- Gutierrez-Arcelus M, Rich SS, and Raychaudhuri S. 2016. Autoimmune diseases - connecting risk alleles with molecular traits of the immune system. *Nat Rev Genet* **17**: 160–174.
- Hayter SM and Cook MC. 2012. Updated assessment of the prevalence, spectrum and case definition of autoimmune disease. *Autoimmun Rev* **11**: 754–765.
- Huang H, Fang M, Jostins L, Mirkov MU, Boucher G, Anderson CA, Andersen V, Cleynen I, Cortes A, Crins F, et al. 2015a. Association mapping of inflammatory bowel disease loci to single variant resolution.

- Huang J, Chen J, Esparza J, Ding J, Elder JT, Abecasis GR, Lee YA, Mark Lathrop G, Moffatt MF, Cookson WOC, et al. 2015b. eqtl mapping identifies insertion- and deletion-specific eqtls in multiple tissues. *Nat Commun* **6**: 6821.
- Jäger R, Migliorini G, Henrion M, Kandaswamy R, Speedy HE, Heindl A, Whiffin N, Carnicer MJ, Broome L, Dryden N, et al. 2015. Capture hi-c identifies the chromatin interactome of colorectal cancer risk loci. *Nat Commun* **6**: 6178.
- Kichaev G, Yang WY, Lindstrom S, Hormozdiari F, Eskin E, Price AL, Kraft P, and Pasaniuc B. 2014. Integrating functional data to prioritize causal variants in statistical fine-mapping studies. *PLoS Genet* **10**: e1004722.
- Lawrie DS, Messer PW, Hershberg R, and Petrov DA. 2013. Strong purifying selection at synonymous sites in *d. melanogaster*. *PLoS Genet* **9**: e1003527.
- Lee S, Teslovich TM, Boehnke M, and Lin X. 2013. General framework for meta-analysis of rare variants in sequencing association studies. *Am J Hum Genet* **93**: 42–53.
- Li Y and Kellis M. 2016. Joint bayesian inference of risk variants and tissue-specific epigenomic enrichments across multiple complex human diseases. *Nucleic Acids Res* .
- Lieberman-Aiden E, van Berkum NL, Williams L, Imakaev M, Ragoczy T, Telling A, Amit I, Lajoie BR, Sabo PJ, Dorschner MO, et al. 2009. Comprehensive mapping of long-range interactions reveals folding principles of the human genome. *Science* **326**: 289–293.
- Liu JZ, McRae AF, Nyholt DR, Medland SE, Wray NR, Brown KM, AMFSI, Hayward NK, Montgomery GW, Visscher PM, et al. 2010. A versatile gene-based test for genome-wide association studies. *Am J Hum Genet* **87**: 139–145.
- Maurano MT, Humbert R, Rynes E, Thurman RE, Haugen E, Wang H, Reynolds AP, Sandstrom R, Qu H, Brody J, et al. 2012. Systematic localization of common disease-associated variation in regulatory dna. *Science* **337**: 1190–1195.
- Mifsud B, Tavares-Cadete F, Young AN, Sugar R, Schoenfelder S, Ferreira L, Wingett SW, Andrews S, Grey W, Ewels PA, et al. 2015. Mapping long-range promoter contacts in human cells with high-resolution capture Hi-C. *Nat. Genet.* .
- Miller AJ. 1984. Selection of subsets of regression variables. *Journal of the Royal Statistical Society. Series A (General)* pp. 389–425.
- Okada Y, Wu D, Trynka G, Raj T, Terao C, Ikari K, Kochi Y, Ohmura K, Suzuki A, Yoshida S, et al. 2014. Genetics of rheumatoid arthritis contributes to biology and drug discovery. *Nature* **506**: 376–381.
- Onengut-Gumuscu S, Chen WM, Burren O, Cooper NJ, Quinlan AR, Mychaleckyj JC, Farber E, Bonnie JK, Szpak M, Schofield E, et al. 2015. Fine mapping of type 1 diabetes susceptibility

loci and evidence for colocalization of causal variants with lymphoid gene enhancers. *Nat. Genet.* .

Pasaniuc B, Zaitlen N, Shi H, Bhatia G, Gusev A, Pickrell J, Hirschhorn J, Strachan DP, Patterson N, and Price AL. 2014. Fast and accurate imputation of summary statistics enhances evidence of functional enrichment. *Bioinformatics* **30**: 2906–2914.

Peters JE, Lyons PA, Lee JC, Richard AC, Fortune MD, Newcombe PJ, Richardson S, and Smith KGC. 2016. Insight into genotype-phenotype associations through eqtl mapping in multiple cell types in health and immune-mediated disease. *PLoS Genet* **12**: e1005908.

Pickrell JK. 2014. Joint analysis of functional genomic data and genome-wide association studies of 18 human traits. *Am. J. Hum. Genet.* **94**: 559–573.

Quinlan AR. 2014. Bedtools: The swiss-army tool for genome feature analysis. *Curr Protoc Bioinformatics* **47**: 11.12.1–11.1234.

Rainbow DB, Yang X, Burren O, Pekalski ML, Smyth DJ, Klarqvist MDR, Penkett CJ, Brugger K, Martin H, Todd JA, et al. 2015. Epigenetic analysis of regulatory t cells using multiplex bisulfite sequencing. *Eur J Immunol* **45**: 3200–3203.

Rao SSP, Huntley MH, Durand NC, Stamenova EK, Bochkov ID, Robinson JT, Sanborn AL, Machol I, Omer AD, Lander ES, et al. 2014. A 3d map of the human genome at kilobase resolution reveals principles of chromatin looping. *Cell* **159**: 1665–1680.

Schofield EC, Carver T, Achuthan P, Freire-Pritchett P, Spivakov M, Todd JA, and Burren OS. 2016. Chicp: a web-based tool for the integrative and interactive visualization of promoter capture hi-c datasets. *Bioinformatics* .

Smemo S, Tena JJ, Kim KH, Gamazon ER, Sakabe NJ, Gómez-Marín C, Aneas I, Credidio FL, Sobreira DR, Wasserman NF, et al. 2014. Obesity-associated variants within fto form long-range functional connections with irx3. *Nature* **507**: 371–375.

Stahl EA, Raychaudhuri S, Remmers EF, Xie G, Eyre S, Thomson BP, Li Y, Kurreeman FAS, Zhernakova A, Hinks A, et al. 2010. Genome-wide association study meta-analysis identifies seven new rheumatoid arthritis risk loci. *Nat. Genet.* **42**: 508–514.

Stergachis AB, Haugen E, Shafer A, Fu W, Vernot B, Reynolds A, Raubitschek A, Ziegler S, LeProust EM, Akey JM, et al. 2013. Exonic transcription factor binding directs codon choice and affects protein evolution. *Science* **342**: 1367–1372.

The Wellcome Trust Case Control Consortium, Maller JB, McVean G, Byrnes J, Vukcevic D, Palin K, Su Z, Howson JMM, Auton A, Myers S, et al. 2012. Bayesian refinement of association signals for 14 loci in 3 common diseases. *Nat. Genet.* **44**: 1294–1301.

- Trynka G, Westra HJ, Slowikowski K, Hu X, Xu H, Stranger BE, Klein RJ, Han B, and Raychaudhuri S. 2015. Disentangling the effects of colocalizing genomic annotations to functionally prioritize non-coding variants within Complex-Trait loci. *Am. J. Hum. Genet.* **97**: 139–152.
- van Berkum NL, Lieberman-Aiden E, Williams L, Imakaev M, Gnirke A, Mirny LA, Dekker J, and Lander ES. 2010. Hi-c: a method to study the three-dimensional architecture of genomes. *J Vis Exp*.
- Wakefield J. 2009. Bayes factors for genome-wide association studies: comparison with p-values. *Genet Epidemiol* **33**: 79–86.
- Wallace C, Cutler AJ, Pontikos N, Pekalski ML, Burren OS, Cooper JD, García AR, Ferreira RC, Guo H, Walker NM, et al. 2015. Dissection of a complex disease susceptibility region using a bayesian stochastic search approach to fine mapping. *PLoS Genet* **11**: e1005272.
- Yang J, Lee SH, Goddard ME, and Visscher PM. 2011. Gcta: a tool for genome-wide complex trait analysis. *Am J Hum Genet* **88**: 76–82.
- Zhu Z, Zhang F, Hu H, Bakshi A, Robinson MR, Powell JE, Montgomery GW, Goddard ME, Wray NR, Visscher PM, et al. 2016. Integration of summary data from gwas and eqtl studies predicts complex trait gene targets. *Nat Genet* **48**: 481–487.